Integration of Wave and Tidal Power into the Haida Gwaii Electrical Grid

by

Susan Margot Boronowski
B.A.Sc., University of British Columbia, 2007

A Thesis Submitted in Partial Fulfillment
of the Requirements for the Degree of

MASTER OF APPLIED SCIENCE

in the Department of Mechanical Engineering

Supervisory Committee

Integration of Wave and Tidal Power into the Haida Gwaii Electrical Grid

by

Susan Margot Boronowski
B.A.Sc., University of British Columbia, 2007

Supervisory Committee

Dr. Andrew Rowe, (Department of Mechanical Engineering)
Supervisor

Dr. Peter Wild, (Department of Mechanical Engineering)
Supervisor

Dr. Brad Buckham, (Department of Mechanical Engineering)
Departmental Member

Abstract

Supervisory Committee
Dr. Andrew Rowe, (Department of Mechanical Engineering)
Supervisor
Dr. Peter Wild, (Department of Mechanical Engineering)
Supervisor
Dr. Brad Buckham, (Department of Mechanical Engineering)
Departmental Member

Rising energy demand, fossil fuel costs, and greenhouse gas emissions have led to a growing interest in renewable energy integration. Remote communities, often accompanied by high energy costs and abundant renewable energy resources, are ideal cases for renewable energy integration. The Queen Charlotte Islands, also known as Haida Gwaii, are a remote archipelago off the northwest coast of British Columbia, Canada that relies heavily on diesel fuel for energy generation. An investigation is done into the potential for electricity generation using both tidal stream and wave energy in Haida Gwaii. A mixed integer optimization network model is developed in a Matlab and GAMS software environment, subject to set of system constraints including minimum operational levels and transmission capacities. The unit commitment and economic dispatch decisions are dynamically solved for four periods of 336 hours, representing the four annual seasons. Optimization results are used to develop an operational strategy simulation model, indicative of realistic operator behaviour. Results from both models find that the tidal stream energy resource in Haida Gwaii has a larger potential to reduce energy costs than wave energy; however, tidal steam energy is more difficult to integrate from a system operation point of view and, in the absence of storage, would only be practical at power penetration levels less than 20%.

Table of Contents

List of Tables

List of Figures

Nomenclature

Tidal Energy

a	amplitude of dominant tidal constituent outside channel in open ocean [m]
A	swept area of turbine [m^2]
c	channel geometry term [m^{-1}]
g	acceleration due to gravity [ms^{-2}]
N	number of tidal stream turbines
P	power [W]
Q	volume flow rate through channel [m^3s^{-1}]
Q_o	volume flow rate in undisturbed state [m^3s^{-1}]
u	flow velocity [ms^{-1}]
η	coefficient of performance of turbine
ρ	density of fluid [kgm^{-3}]
λ_1	turbine drag parameter
ω	frequency of dominant tidal constituent outside channel in open ocean [s^{-1}]

Wave Energy

a	wave amplitude [m]
a_{rms}	root mean square of displacement of water surface of wave from mean position [m]
c	wave speed [ms^{-1}]
c_g	wave group velocity [ms^{-1}]
d	wave depth [m]
E	total energy of a wave [J]
h	displacement of water surface of wave from mean position [m]
H	wave height [m]
$H_{1/3}$	“one third” significant wave height [m]
H_s	significant wave height [m]
N_c	total number of wave crests
P	wave power [Wm^{-1}]

T	wave period [s^{-1}]
T_c	mean crest period [s^{-1}]
T_e	wave energy period [s^{-1}]
T_p	peak wave period [s^{-1}]
T_z	mean zero crossing wave period [s^{-1}]
λ	wavelength [m]
ζ	coverage factor

Network Model

c	cost [CAD]
e	CO_2 emissions from generation [$kgCO_2MWh^{-1}$]
E	total generation of CO_2 emissions for period T [$kgCO_2$]
g	incremental production cost [$\$MWh^{-1}$]
G	power generation at a bus [MW]
K	number of cost levels
KS	Kolmogorov-Smirnov test statistic
L	power consumption at a bus [MW]
$Loss$	power loss across a bus connector [MW]
M	incremental generation for a cost level [MW]
P	power entering or leaving a bus connector [MW]
Pop	population of a network
R	resistance of a bus connector [Ω]
$Sink$	power sink at a bus [MW]
V	voltage of a bus connector [V]
w	variable indicating a diesel generating unit started up
x	state variable of a diesel generating unit
y	percent of incremental generation used for a set cost level
z	variable indicating a diesel generating unit shut down

Superscripts

*	non-dimensional value

Subscripts

cap	nameplate capacity of a generator
d	dispatchable generator index
i,n	bus indices
j	bus connector index
k	cost level index
loc	location
m	month
maint	maintenance
max	maximum
min	minimum
sd	diesel generating unit is shut-down
su	diesel generating unit is start-up
t	discrete time index
T	total time steps
Tot	total
y	year

Abbreviations

CD	Central Dixon Entrance buoy location
CDF	cumulative distribution function
CF	capacity factor
CPUC	California Public Utilities Commission
EMEC	European Marine Energy Test Centre
EPRI	Electric Power Research Institute
FERC	Federal Energy Regulatory commission
GAMS	General Algebraic Modeling System

IPP	independent power producer
MEDS	Marine Environmental Data Services
O&M	operation and maintenance
PG&E	Pacific Gas and Electric Company
PPA	power purchase agreement
SCDF	empirical cumulative distribution function
TE	tidal energy
TP	tidal plant
WEC	wave energy converter
WM	West Moresby buoy location

Acknowledgments

First and foremost, I would like to thank my supervisors, Drs. Andrew Rowe and Peter Wild, for their support, guidance, and contributions to this work. A special thank you is owed to Dr. G. Cornelis van Kooten, Jesse Maddaloni, and Justin Blanchfield for all of their much appreciated assistance, expertise, and patience. Additionally, thank you to my fellow graduate students, Torsten Broeer, Scott Beatty, and Clayton Hiles, who were always there to offer help and encouragement when needed.

Chapter 1

Introduction

Electricity generation is an issue of increasing interest due to growing energy demand, fossil fuel costs, and greenhouse gas emissions. This issue is of particular concern to remote communities, where the cost of electricity is generally higher than the norm [1]. The Queen Charlotte Islands, also known as Haida Gwaii, are a remote archipelago off the northwest coast of British Columbia, Canada with an isolated electricity generation system that is heavily dependent on diesel fuel for operation [2]. Currently, there are two separate grids on Haida Gwaii, north and south, each supplying approximately 1500 customers [2]. The peak load for the north grid in 2005 was roughly 4.8 MW, just under 1 MW less than that of the south grid [3]. A small hydro power facility, sized at 5.7 MW, exists in conjunction with two diesel generation systems, sized at 9.15 and 11.4 MW [3], resulting in a system average cost of electricity production in 2006 of 0.26 $/kWh [2].

A potential option to reduce the cost of electricity for the region, as well as greenhouse gas emissions, is to incorporate some form of renewable energy into the system. A resource of particular interest to jurisdictions along a shoreline is ocean energy. Haida Gwaii is strategically located with lengthy coastlines that offer generous amounts of wave and tidal energy. Estimates from the National Research Council suggest the mean annual wave power available near the western shore of Haida Gwaii to be on the order of 45 kW/m, while estimates for exposed sites in deep water are even higher at approximately 54 kW/m [4]. Triton Consultants, who were commissioned by the National Research Council, estimate the mean potential tidal current energy in the Haida Gwaii region to be 81 MW. This tidal current energy potential is distributed among 9 different sites, the largest of which is Masset Sound with a 21 MW potential [5].

Renewable energy sources including wind, solar, wave, tidal stream, and run-of-river hydroelectric are considered *non-dispatchable* as they cannot be called upon to increase their output if needed. However, energy output from these sources can be curtailed. Traditional generators, such as diesel, thermal and large scale hydroelectric

plants, are considered *dispatchable* due to the fact that output can be increased at the system operator's command.

A major issue with renewable energy sources is their intermittent nature. Short term fluctuations in power from these sources, combined with fluctuations in demand, create a difficult environment for the generation system to meet the load [1]. Renewable energy is often considered *must-take*, indicating that if it is available it must be used by the system [6]. Sudden fluctuations in renewable energy cause traditional dispatchable generators to ramp up or down quickly to meet the load. Furthermore, these generators are forced to be ready to meet the load in the case of a drop in renewable power, thereby increasing system balancing reserve [7]. Another impact is the reduction of generator efficiency as a result of often being forced to operate at lower part loads [1]. Tidal stream power has the advantage of being completely predictable due to the cyclical nature of the tides; however, it is still intermittent. Waves, on the other hand, are only predictable on the short term, although seasonal variability can be predicted long in advance [4].

In order to understand the impact of incorporating renewable energy into the generation system in Haida Gwaii, from system operation, cost, and emissions perspectives, it was necessary to build a network model. This type of energy system modeling is well developed with many papers discussing supply and demand analysis, new energy sources integration, as well as energy transmission [8]. The following section will review the area of energy system modeling, followed by a discussion of studies considering the impacts of integrating renewable energy. Finally, the objective and scope of this thesis will be defined.

1.1 Energy System Modeling

Energy system modeling is a broad, well developed field, from which many different types of models have emerged. Some of the main types include energy planning models, energy supply-demand models, forecasting models, neural network models and emission reduction models. Jebaraj and Iniyan [8] present an extensive review of such models.

Energy planning models, also referred to as integrated energy system models, often incorporate optimization techniques in order to find the lowest cost solution. Such models include that developed by Joshi, where a schedule for a supply system consisting

of a mix of energy sources and conversion devices for a typical village in India was developed with the goal of minimizing cost [9]. Malik similarly designed a planning approach for the Wardha district in India, using a mix of new and conventional energy technologies in a mixed integer linear optimization model [10]. Other models include multi-objective, quadratic and linear programming methods [8].

Energy planning models can obviously include renewable energy in the system that is being analyzed. Iniyan and Sumathy built such a model, where the cost/efficiency ratio was minimized while determining the optimum allocation of different renewable energy sources for various end uses. Constraints in their analysis included energy demand, potential of renewable energy sources, and reliability and acceptance of renewable energy systems [11]. A wind-hydro system model, which determined the optimal configuration of a proposed renewable energy development for several typical Agean Sea Island cases, was developed by Kaldellis and Kavadis. Long term wind speed measurements, electrical load demand and system operational characteristics were included in the analysis [12].

Energy system planning often means the scheduling of fossil-fuel power generation systems. The two main decisions that a system operator must make include the *unit-commitment* and *economic dispatch* decisions. The unit-commitment decision, which decides if a generating unit will be in operation at each point in time, must consider generator capacity requirements such as minimum and maximum operational levels and the cost of starting up or shutting down a generating unit. The economic dispatch decision ensures that load is met by some configuration of generating unit operation, which depends on relative efficiencies of the units. Therefore, scheduling of an energy system to minimize cost must be done by simultaneously considering the unit commitment and economic dispatch decisions. This is done at once for all time periods analyzed, usually sized at 1 hour. This is known as dynamic optimization, which enables the system to look forward and backward in time when deciding which generating units to operate. [13]

Economics are the basis of supply-demand models, where the impacts on energy supply and demand are considered in conjunction with other factors. An example of this

is a study done by Uri (1985) in which the impact that prices and economic activity have on demand for gasoline in the US was analyzed [14].

Forecasting models, used to determine future energy distribution patterns, include variables such as population, income, price, growth factors, and technology. These models can be developed for commercial, as well as renewable, energy systems. Uri (1978) developed an econometric time series forecasting model that predicted monthly peak system load [15], and Wisser predicted the wind energy potential of Grenada based on historic readings of mean hourly wind velocity [16].

Other energy models include those based on neural networks and emission reduction. Neural network models utilize fuzzy logic to rank the relative importance between supply and demand determinants [8]. Emission reduction models include climate system models and individual energy system models where the impact on emission reduction is the focus [8]. An example of an emission reduction model is a multi-objective optimization model built by Hsu and Chou to determine the impact of energy conversion policy on the cost of reducing carbon dioxide emissions in Taiwan [17].

1.2 Integration of Renewable Energy into Electrical Grids

The issue of intermittency is of significant concern for widespread adoption of renewable power. Fluctuations in power output due to changing resources can have a negative impact on system operation as well as power quality [1]. To maintain power quality, traditional generation is forced to match the power fluctuations from renewable sources through increased ramping, leading to lower overall fuel efficiencies and increased maintenance. Generation responsiveness and grid strength determine the viable level of intermittent capacity that can be installed in a grid [1].

A report by Gross et al. [7] showed that system balancing reserves and system margin are two areas where the effect of intermittent renewable energy can also be seen. System balancing reserves deal with unexpected short term fluctuations on the order of seconds to hours. Sized on a statistical basis according to the expected range of unpredictable variation in demand, reliability of generators and scale of a potential fault, their purpose is to maintain a low risk of demand being unmet. System margin is the difference between installed generation capacity and peak demand. It is sized according

to the number of, and reliability of, generators as well as variability in demand. Intermittent renewable energy sources increase the supply uncertainty and therefore both system balancing reserves and system margin requirements also increase, adding to the cost of electricity generation for the system.

Autonomous systems greater than 1 kV and less than 50 kV have been shown to successfully absorb instantaneous wind power penetration up to 40% without special control measures [1]. This means that at a specific point in time 40% of the load is being met by wind power. Due to their small scale, autonomous grids do not benefit from geographically distributed wind. Where distributed wind acts to smooth overall wind power in a large system, no smoothing occurs in an autonomous system. This intermittency, combined with system operating constraints, can limit the possible penetration of wind power without control mechanisms in place. However, the need for control can be minimized with the use of rapid response complementary power plants, such as gas or hydro. Multiple measures can be taken to further increase wind penetration including grid reinforcement, inclusion of storage, wind velocity forecasting, and voltage-controlled power production, whereby power spikes are mitigated via thyristors that gradually connect the turbines to the grid [1]. This method of voltage control has been shown to achieve 100% wind penetration at times while maintaining voltage stability of the grid [1].

Autonomous grids with wind-diesel systems are seen throughout the world. One such example is Cape Verde, where grid control is performed manually by diesel plant operators for instantaneous power penetration levels up to 35% with no serious technical problems. Ten Mile Lagoon, Australia is another example, where a 33 kV grid has nine 225kW wind turbines that contribute 10% of the annual energy demand. Instantaneous wind power penetration is kept below 40% at all times by feathering the blades of the turbines. However, under test conditions, penetration was allowed to reach 60% and showed no adverse effects on system stability. This level of instantaneous power penetration cannot be maintained because stability cannot be guaranteed. In 2005, wind power in Crete, Greece, another autonomous grid, contributed approximately 10% of the electricity demand with maximum instantaneous power penetration reaching 40%. [1]

Wind-diesel systems for remote communities in Canada have been implemented since the 1980s [18]. Unfortunately, these systems have been largely unsuccessful due to cost overruns linked to operation and maintenance of the wind generators [18]. A study done by Weis and Ilinca [18] considered typical small and medium remote Canadian communities where the maximum loads were 260 kW and 700 kW, respectively. They found that without storage the optimal number of turbines, sized at 65 kW each, was 5 for the small and 10 for the medium community. This corresponds to power penetration levels of 125% and 93%, respectively, where power penetration is defined as installed wind capacity divided by peak load. Due to issues with intermittency, the optimum number of turbines did not increase indefinitely with increasing wind speeds. However, including idealized energy storage doubled the optimal number of turbines in both cases.

Kaldellis [19] studied the maximum wind energy penetration in the Aegean Archipelago, where multiple autonomous island grids exist. There is excellent wind potential in this area, with the annual mean wind speed exceeding 5.5m/s. Additionally, the electricity production cost is extremely high with insufficient power supply problems often encountered. Kaldellis found that the maximum wind energy contribution for excellent wind potential areas was 20%, with this value dropping to 15% for average wind potential areas. Only with the addition of storage would the level of wind energy input be able to increase above these levels, despite the abundant wind resource.

Another major barrier for adoption of renewable power is capital cost. Maddaloni et al. [20] built a load balance model where wind was integrated into three different generation mixtures, all with the same load profile. They considered a hydro dominated mix, coal dominated mix, and an equal parts hydro and natural gas mix. The cost of electricity was found to increase for all cases due to the high capital cost of wind power. More importantly, it was found to increase the most for the hydro dominated mix and the least for the equal part hydro and natural gas mix. This was due to low fuel costs being mitigated in the hydro case as opposed to relatively high costs in the natural gas case.

Bakos [21] considered a hybrid wind/hydro power system for the island of Ikaria, Greece where the maximum and minimum demands were 4020 kW and 800 kW, respectively. The power for the isolated grid on Ikaria is currently generated through the use of diesel and mazut. The proposed hybrid system would combine a wind farm with a

reversible-hydro power station and a parallel water pump station. The study found that the cost of electricity could drop 0.05 $/kWh from 0.17 $/kWh to 0.12 $/kWh with the installation of 14 wind turbines, although no mention of capital cost is included.

1.3 Thesis Objective and Outline

The objective of the following research was to analyze the effects on the Haida Gwaii generation system when highly variable wave and tidal stream power were added to the existing dispatchable generation system. A mixed integer optimization model was built to determine the minimum cost solution, results from which were used to develop a more realistic operational policy. Constraints such as generator response time, part-load efficiencies, capacities, and minimum operational level, as well as transmission line capacities, were included with the aim of realistically representing the network. The existing grid was modeled along with a proposed linked grid structure, where the two grids are linked at their nearest point. The effects on system operation, cost and emissions for both grid structures with varying levels of installed wave and tidal capacity were determined.

This thesis will begin by reviewing the resource potential of both tidal and wave power in the Haida Gwaii region. The theory behind tides and tidal stream power will be reviewed, along with its potential in Haida Gwaii. This will be followed by a detailed discussion of wave power and its potential in the region as well. Following the wave resource quantification for Haida Gwaii, the existing network will be introduced and the optimization network model that was built will be discussed. All aspects of the optimization model will be detailed, including constraints, costs, input data and model parameterization. Optimization model results for linking the grids, as well as integrating tidal and wave power, will be presented and discussed, from which a simulation model outlining an operational control strategy for the system will be developed. The effects of integrating tidal and wave power into a system controlled by such an operational strategy will be analyzed in order to represent more realistic operator behaviour and system impacts. Finally, simulation results for both tidal and wave power integration will be compared to one another, helping to determine the best renewable energy option for Haida Gwaii.

Chapter 2

Potential for Tidal Stream Power in Haida Gwaii

The high cost of electricity in Haida Gwaii has led to significant interest in incorporating renewable energy into the generation mix. One resource that has been considered is tidal power, with several reports investigating the tidal stream power potential in the area [5, 22]. The following chapter will review the theory behind ocean tides and several studies that have estimated the potential tidal stream power available in the Haida Gwaii region.

2.1 Background

Tides are generated from the gravitational forces of over 400 celestial bodies. Of those bodies, the sun and moon are the most important. Although the mass of the sun is far greater, the tide generating force from the moon is twice that of the sun. This occurs because the tide generating force is inversely proportional to the cube of the distance from the center of the earth to the center of the tide generating object. It follows, therefore, that the tidal pattern is primarily a result of the rotation of the earth and the moon about their common center of mass, located 1600 km beneath the surface of the earth. Gravitational forces and the centripetal force acting on all particles of the earth combine to produce a net force that creates two tidal bulges, one towards the moon and the other away from the moon. This bulge shifts its position on the surface of the earth as it rotates about its axis. Since the earth-moon system is rotating about each other while the earth is rotating about its axis, the moon moves 12.2˚east of a stationary observer on the surface of the earth after a solar day of 24 hours. An extra 50 minutes is required to match the location of the observer directly in line with the moon, thereby identifying the lunar day of 24 hours and 50 minutes. [23]

Tides follow the same time period as a lunar day; however, tides are further complicated by the sun's gravitational force. When the moon is between the earth and the sun, it is said to be in conjunction; when it is on the opposite side of the earth from the sun, it is said to be in opposition. If the moon is at a right angle to the sun relative to the earth it is said to be in quadrature. When the moon is in either conjunction or opposition, the gravitational forces from the sun and moon combine, thereby producing

maximum tidal ranges. These tides are referred to as spring tides. When the moon is in quadrature, the gravitational forces from the sun and moon are at right angles to each other. This results in the minimum tidal range, referred to as a neap tide. The earth moon system is in the same phase with respect to the sun every 29.5 days, resulting in a 15 day cycle of spring and neap tides. [23]

The declination of both the earth and moon are another aspect affecting the tides. As the earth revolves around the sun, its axis of rotation is tilted 23.5˚from vertical relative to its orbital path, creating the four seasons. Furthermore, the moon's orbit is at an angle of 5˚relative to the earth's orbital path. This means the tidal bulges are rarely aligned with the equator, but rather lie at any latitude from the equator to 28.5˚on either side. In most cases, successive high and low tides have different amplitudes, called the diurnal inequality. In fact, the tides are only further complicated by the many other tide generating variables called partial tides. All of these celestial forcings combined cause the tides to repeat themselves every 18.6 years. [23]

Equilibrium theory of tides, as described above, assumes the earth has a smooth surface completely covered with water. In reality, tides are altered by the presence of continents and ocean basins of varying depths, sizes and shapes. Tides are classified as diurnal, semi-diurnal, or mixed. Diurnal indicates a single high and low tide each lunar day, while semi-diurnal refers to two high and two low tides of approximately the same amplitude each lunar day. A mixed tide combines aspects from both diurnal and semi-diurnal tides. They most commonly have a semi-diurnal period, although that is not always the case, and often have large variation in amplitude of successive high and low tides. This type of tide is the most common tide seen throughout the world and also Haida Gwaii. [23]

Tidal streams are horizontal currents created from the motion of the tides. Tidal streams associated with the rising and falling of the tide are referred to as the flood and ebb, and have an almost uniform velocity throughout the entire depth of water. Slack water occurs during the short time interval between the end of the flood and the beginning of the ebb, or vice versa, when there is no horizontal motion of the water. Tidal stream velocities measured along the British Columbia coast range from 0.5 m/s in the open ocean to approximately 8 m/s at Nakwakto rapids. Although tidal streams are

directly related to the tides, the strength of the current does not necessarily coincide with the amplitude of the corresponding vertical change. Tidal stream power uses these tidal streams to turn a turbine, much in the same way that wind is used to power a wind turbine. [24]

2.2 Resource Assessment

Tidal stream resources are often reported according to the average output power over temporal fluctuations, known as the mean power. The annual mean power is, therefore, the average value of output power over an entire year. Another common way of characterizing a potential site is to calculate its mean power density, the mean power per unit area. While mean power represents the total power potential of a site, the mean power density represents the power intensity of the flow. [4]

A recent study undertaken by Hatch Energy [22] estimates the mean potential tidal power available in Haida Gwaii to be 88.7 MW. Of the 88.7 MW estimated, 21.5 MW of that is assumed to be from a site located in Masset Sound. Triton Consultants [5] similarly estimates the mean potential power of the region to be 81 MW, with 14 – 27 MW of that value coming from a site also selected in Masset Sound. Both of these estimates were based on the energy flux method:

$$P = \frac{1}{2} N \eta \rho A_{turb} u^3, \tag{1}$$

where P is power available in watts, N is the number of turbines present, η is the coefficient of performance of the turbine unit, ρ is the density of the fluid (kg/m^3), A_{turb} is the swept area of the turbine blades (m^2), and u is the velocity of the fluid (m/s) [5]. However, it has been shown that the maximum extractable power is not directly related to the undisturbed kinetic energy flux of the flow as assumed by this method [25]. In fact, Triton admits that "…kinetic energy is only loosely related to the extractable power since extractable power is highly dependent on the physical characteristics of the site…" [5].

Recent work by Garret and Cummins [26] has considered a channel linking two large basins while including the effects of flow acceleration, bottom drag and exit separation that were previously neglected. This work was furthered by Blanchfield et al. [27] who analyzed the case of a bay linked to the open ocean by a channel, using Masset

Sound, Haida Gwaii as a case study for the model. Blanchfield et al. found that the maximum average extractable power in Masset Sound, P_{max}, can be expressed as

$$P_{\max} = 0.21\rho g a Q_0, \tag{2}$$

where ρ is the water density, g is acceleration due to gravity, Q_0 is the maximum volume flow rate in the undisturbed state, and a is the amplitude of the dominant tidal constituent outside the channel in the open ocean. Instantaneous power was expressed as

$$P = P^* \rho \frac{(ga)^2}{c\omega}, \tag{3}$$

where c is the channel geometry term and ω is the frequency of the dominant tidal constituent. P^* is the non-dimensional extractable power, expressed as a function of the turbine drag parameter λ_1^* and non-dimensional flow rate Q^* as

$$P^* = \lambda_1^* Q^{*2} \left| Q^* \right|. \tag{4}$$

Results from this case study suggest a maximum average extractable power of 87 MW is available in Masset Sound; however, extraction of this amount would reduce the volume flow rate through the channel to approximately 58% of the undisturbed state. It was found that limiting the average power extracted to approximately 37 MW would reduce the volume flow rate through the channel by 10%, a more acceptable level. These values represent the maximum average extractable power and are, therefore, significantly higher than estimates based on the energy flux method. [27]

Chapter 3

Potential for Wave Power in Haida Gwaii

Another resource that has been considered for integration into the Haida Gwaii grid is wave power. In order to determine a typical annual hourly wave power profile, data from buoys in the ocean surrounding Haida Gwaii was analyzed; however, the theory behind wave energy first needs to be understood in order to utilize the buoy data. The next section briefly outlines the theory behind wave energy, followed by a review of three wave energy conversion devices currently being developed. Wave data from five buoys is analyzed, theoretical wave power is determined, and the buoy data is combined with power capture matrices from the wave devices analyzed to determine hourly wave energy available in a given year for each device. Each location is then assessed according to the average annual capacity factor and location relative to the grid.

3.1 Wave Energy Background

Waves are generated when a disturbance, such as wind or a passing boat, forces particles of water out of their equilibrium state. In response, gravity acts to restore equilibrium, but overshoots due to the inertia of the water and must correct again. Once again the correction is overshot, and the cycle continues at regular intervals of time. This behaviour is very similar to the swinging of a pendulum. [24]

Free surface waves are characterized by certain properties: wave period, wave speed, wavelength, and wave height. Wave period, T, is the time it takes two successive crests to pass a fixed point, whereas wave speed, c, is the speed of the wave relative to a fixed point [24]. Wavelength, λ, is the distance from one crest to the next, and wave height, H, is the distance from trough to crest of the wave [24]. Other well known properties include wave amplitude, a, and water depth, d. Wave amplitude is the distance from the mean water line level to the trough or crest of a sinusoidal wave, equal to half the wave height, whereas water depth is the distance from the mean water line level to the base of the column of fluid.

3.1.1 Classification

Waves are often classified as deep, intermediate or shallow. Deep water waves are characterized by a water depth greater than ¼ of their wavelength. These types of waves

are usually wind waves or swell in the open ocean and are not affected by the bottom topography. Intermediate water waves occur when the water depth is between ¼ and 1/20 of their wavelength. A common intermediate water wave is swell at the continental shelf from the open ocean. These waves are only partially affected by the bottom topography. Shallow water waves occur when the water depth is less than 1/20 of their wavelength and they are strongly influenced by bottom topography. Shallow water waves include tides and tsunamis as these both have very long wavelengths. [24]

Water particle motion differs for deep, intermediate and shallow water waves. Particles in a deep water wave move in a circular motion with a radius of motion that deceases exponentially with depth. Shallow water wave particles move in ellipses near the surface, flattening to straight lines near the bottom. Unlike deep water waves, where particle movement degrades to zero with depth, the horizontal movements of shallow water waves decrease only slightly with depth. This is seen practically in tidal currents in open water, a classic shallow water wave, where velocity is almost uniform throughout the column of water. [24]

Waves can also be classified according to their period. Table 1 shows various types of waves described by their primary generating and restoring mechanisms. Gravity waves are the type of wave focused on for wave energy production.

Table 1: Basic types of surface waves according to period [24]

Name	Periods	Wavelengths	Generating Mechanism	Restoring Mechanism
Capillary waves (ripples, wavelets)	Less than 0.1s	Less than 2 cm	Wind, pressure fluctuations	Surface tension
Gravity waves (chop, sea, swell)	0.5 – 30 s	10 cm – 1000 m	Wind	Gravity
Infragravity waves	Minutes	Hundreds of meters to hundreds of kilometers	Storm systems	Gravity
Tsunamis	Tens of minutes to 1 h	Hundreds of kilometers	Submarine earthquakes, shoreline slumping	Gravity
Tides	Mainly 12.5 and 25 h	Thousands of kilometers	Gravitational attraction of sun and moon	Gravity and coriolis force

3.1.2 Power Extraction from Waves

Elementary theory of deep water waves starts by considering a regular wave of sinusoidal shape. Wave theory is complex and it is not the intention of this report to delve into theory, but to extract and present the pertinent details. Energy of a wave is found by summing the kinetic and potential energy contained in each particle of the wave. Power in that wave, P, is represented in terms of kW per meter of wave crest width by

$$P = Ec_g, \tag{5}$$

where E is the total energy of the wave and c_g is the velocity at which the energy of the group of waves moves forward, known as group velocity [28]. In deep water, group velocity is equal to ½ the individual wave speed [24]. In terms of wave properties, power is equal to

$$P = \frac{\rho g^2 a^2 T}{8\pi}, \tag{6}$$

where ρ is density of the fluid, g is gravitational acceleration, a is wave amplitude, and T is wave period [28].

In reality, wave systems are made up of multiple waves with varying amplitude, period and direction. Swell, a commonly used term, refers to wave trains in a preferred direction with a long period, generated by a continuous wind [24]. Inconsistent winds lead to shorter period waves with erratic motion, called a sea [24]. In order to understand the wave environment in a particular location, data must be collected over many different sea states or a long period of time. When doing so, certain values are tracked including: N_c, $H_{1/3}$, H_s, H_{max}, T_z, T_p and T_c. In a set time period, N_c represents the total number of crests, $H_{1/3}$ the 'one third' significant wave height (average height of the highest 1/3 of the waves), and H_s the 'true' significant wave height represented by

$$H_s = 4a_{rms} = 4\left[\frac{\left(\sum_{i=1}^{n} h^2\right)}{n}\right]^{\frac{1}{2}}, \tag{7}$$

where a_{rms} is the root mean square of the displacement of the water surface from the mean position (h), calculated from n measurements at equal time intervals [28]. H_{max} is

the maximum height of a wave; T_z is the mean zero crossing period, calculated by dividing the total time of the record by the number of upward crossings of the mean water level; T_p is the peak period, or most energetic wave period at a specific point; and T_c is the mean crest period, or duration of record divided by N_c. [28]

Power from real waves is often represented in terms of H_s and the energy period, T_e. The energy period is the period of a single sinusoidal wave with the same energy as the sea state [4, 28]. Power from a wave is represented by

$$P = \frac{\rho g^2 H_s^2 T_e}{64\pi}. \tag{8}$$

The energy period is rarely specified; however, for many seas $T_e = 1.12\ T_z$ [28]. If T_p is known, it is assumed that $T_e = \alpha T_p$, where $\alpha = 0.86$ for a Pierson-Moskowitz spectrum and increases towards unity with decreasing spectral width [4].

3.2 Wave Energy Conversion Devices

As wave energy conversion is a developing industry, many wave energy converters (WEC) exist in the pre-commercial phase. A common way of classifying WEC devices is according to their alignment to oncoming waves. Three types of devices exist: point absorbers, terminators, and attenuators. Point absorbers are devices similar to buoys in that they are usually axisymmetric about a vertical axis and have a small horizontal dimension compared to the wavelength of incoming waves. These devices are able to absorb energy from a large range of wavelengths with any directionality, limited only by the allowable magnitude of device oscillations. Attenuators and terminators, on the other hand, have one dominant horizontal dimension. Attenuators are aligned with the incoming wave direction so their beam is much smaller than their length. Terminators are the opposite of attenuators and have their dominant direction perpendicular to the incoming waves, meaning their beam is much larger than their length. Although similar in design, mooring forces are much larger for terminators than attenuators due to their alignment relative to incoming waves. [29]

Further device classification is often done according to location of the device and form of energy conversion. Device location is categorized as offshore, onshore or nearshore, with offshore indicating depths greater than 50 m. Wave energy can be converted to hydraulic, pneumatic or mechanical energy, or converted directly to

electricity. Hydrualic energy is the pressurization of a liquid, typically water or oil, via wave driven pumping. This pressurized fluid is sent to a tank or reservoir from which it exits at a constant rate to drive a turbine or other hydraulic motor. This way the output power can be smoothed and controlled according to the rate of fluid leaving the tank. In the case that the fluid is sea water an open loop system is possible. Pneumatic systems pressurize a gas rather than a liquid, with air being the typical gas used. Conversion directly to mechanical energy was typical of 19th century WEC devices; however, this type of energy conversion system is not seen anymore. Direct conversion to electricity, although possible, is often considered undesirable due to the fluctuating output from the wave motion. [29]

The focus of this report will be on offshore WEC devices. Three devices have been chosen: a point absorber, attenuator and terminator. The chosen point absorber, attenuator and terminator are AquaBuOY, Pelamis and Wave Dragon, respectively. AquaBuOY is owned by Finavera Renewables Ltd., Pelamis by Pelamis Wave Power Ltd., and Wave Dragon by Wave Dragon Ltd.

3.2.1 AquaBuOY

AquaBuOY, as the name sounds, is a floating buoy structure categorized as an offshore point absorber with hydraulic energy conversion. The AquaBuOY device contains four main elements: buoy, acceleration tube, piston and hose pump (Figure 1). A cylindrical buoy, 6 m in diameter [30], acts as a float, or wave follower. Rigidly attached to the underside of the buoy is a vertical hollow cylinder 30 m in length [30] that is open to the water on both ends, allowing water to pass back and forth as the float follows the surface. Midway in the tube is a neutrally buoyant piston that moves up and down due to the water moving through the tube. The hose pump is a steel reinforced rubber hose whose internal volume is reduced when the hose stretches. Two hose pumps are used in the design, each attaching from one end of the acceleration tube to the piston. When the piston moves within the tube the hoses stretch and compress. The stretching hose pressurizes the sea water within it, which is then fed to a high pressure accumulator. Pressurized seawater from the accumulator is subsequently fed through a turbine that drives a generator. Electricity from that generator is brought to shore via a standard submarine cable. [31]

Survivability of devices in extreme weather is a main concern for wave device developers. This issue is often referred to as the end-stop problem. In the case of extreme weather, the piston assembly in the AquaBuOY will move into an area where the hose pump will widen. This enables the water inside the tube to bypass the piston assembly, effectively discharging the fluid without putting stress on the system. [31]

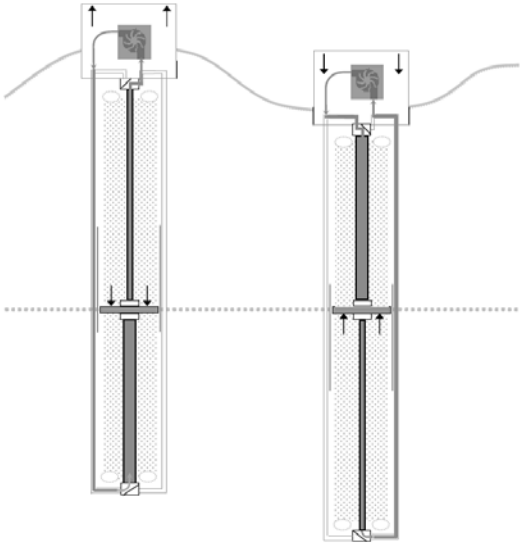

Figure 1: AquaBuOY operating principle [32]

Sea trials of AquaBuOY's predecessor, the IPS buoy, were performed in the North Sea in 1981 [30]. The IPS buoy has the same hydrodynamic design but a different power take off system [30]. Numerical modeling was carried out by AquaEnergy, the first developers of AquaBuOY, in 2003 along with initial planning for a pilot plant in Makah Bay, Washington that included wave tank testing at Aalborg University [30]. June 2006 saw the acquisition of AquaEnergy by Finavera Renewables Ltd [33]. This was followed by the deployment of AquaBuOY 2.0 on September 6, 2007 3.5 miles off the coast of Newport, Oregon [33]. AquaBuOY 2.0 was the first installation of a WEC of this scale on the west coast of North America [33]. However, on October 27, 2007 the prototype that had been designed to last three months sank, one day before it was scheduled to be removed from the water [34]. Throughout the period the prototype was being tested, mathematical and power output modeling was verified [33].

Following the deployment of AquaBuOY 2.0, Finavera Renewables focused on a third generation buoy, AquaBuOY 3.0, while narrowing their focus to the west coast of

North America and South Africa. Additionally, they signed a long term power purchase agreement (PPA) with Pacific Gas and Electric (PG&E) for a 2 MW project off the coast of California, scheduled to be the first commercial PPA for wave energy in North America. However, in October 2008 the California Public Utilities Commission (CPUC) denied PG&E's application for a PPA. In February 2009 Finavera Renwables announced it was surrendering its Federal Energy Regulatory Commission (FERC) licence for the Makah Bay wave energy pilot project in Washington and was focusing solely on wind project development. [33]

3.2.2 Pelamis

The Pelamis device is a floating structure composed of multiple cylindrical sections linked together, giving it the semblance of a snake. Classified as an attenuator and offshore device, it is held in place by a mooring system that allows it to align itself parallel to the direction of travel of oncoming waves. The hinged joints linking the sections of the device together flex as a wave travels down the length of the device and it heaves and sways. This motion of the joints drives hydraulic rams that pump high pressure biodegradable hydraulic fluid to an accumulator. From there it is run through a hydraulic motor at a constant rate that in turn drives an electrical generator. Should a leak occur, the hydraulic fluid is able to decompose completely within a few days.

The accumulators are sized in order to provide continuous, smooth output power comparable to that of a conventional generator. Power from all joints in the device is sent down a single cable to the seabed where it meets up with power from other devices and is sent to shore via a seabed cable. In the event of extreme weather or loss of the grid, excess power can be dumped via a heat exchanger included in each device. Mechanical to electrical power conversion efficiency ranges from 70 – 80% depending on the sea state, where maximum efficiency is achieved at rated capacity. [29]

The Pelamis can be installed in a range of water depths and bottom conditions, allowing for site variability. The device is constructed and assembled on land from "off the shelf" components and towed to the desired location. Once on location, rapid attachment/detachment electrical and mooring connections minimize set-up costs. Additionally, it can be moved easily for future maintenance. These design features are intended to keep operational costs low. [29]

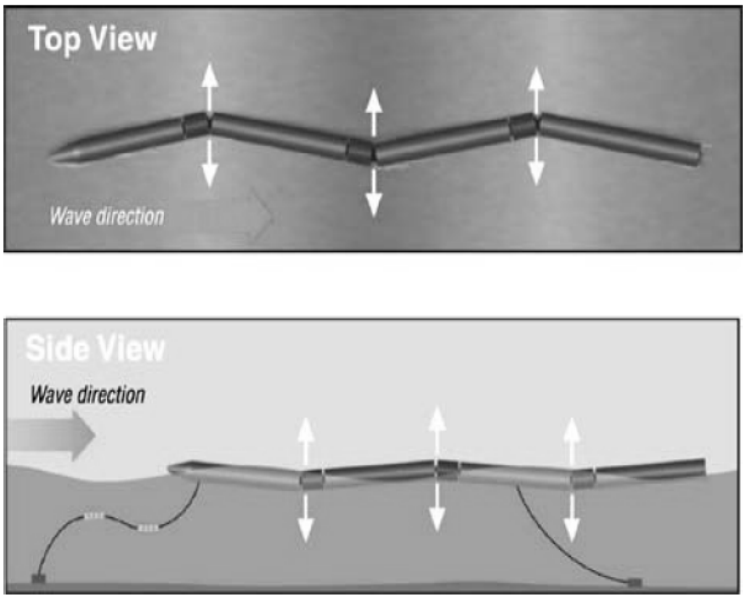

Figure 2: Pelamis device [35]

A full scale pre-commercial prototype rated at 750 kW was first deployed in early 2004 in the North Sea where it underwent sea trials. In August of 2004 the prototype was towed to the European Marine Energy Test Centre (EMEC) in Orkney, Scotland, where power produced was supplied to the local grid. Following this success, the Electric Power Research Institute (EPRI) reported that Pelamis was the only WEC technology suitable for immediate deployment [30]. In 2006 the prototype was removed from EMEC to check for any problems and to upgrade the device to the newest design, the P1A Pelamis. Further sea tests were subsequently carried out on the upgraded prototype before it was reinstalled at EMEC in March of 2007. [29]

In 2005, three P1A machines were ordered by a Portuguese Consortium led by Enersis for the world's first multi-unit wave farm [29]. This was also the world's first commercial order for WECs [36]. The wave farm, Aguçadoura, was to be located 5 km offshore on the north coast of Portugal [29]. Additionally, Enersis issued a letter of intent for purchases of another 20 MW of Pelamis devices [36]. Following this initial agreement, in December 2008 Enersis was purchased by Babcock and Brown, an Australian infrastructure company [36]. The wave farm continued to be supported and in September 2008 Pelamis Wave Power successfully commissioned the first three units [36]. The machines were later removed to resolve engineering related issues with regards

to the location of the machine's bearings in their housings [36]. In late 2008, Babcock and Brown encountered financial trouble and the project stalled while waiting for a new partner [36]. It is the view of Pelamis Wave Power that the machines will be ready for redeployment when a new partner is found [36].

3.2.3 Wave Dragon

Wave Dragon is a floating, terminator type, overtopping device (Figure 3). Designed for water depths greater than 20 m it can be classified as a nearshore or offshore device. Two arms focus the waves towards a double curved ramp and increase the wave height substantially in doing so. Once the water moves up the ramp it spills into the overtopping basin, a concrete reservoir. Water exits the reservoir through multiple low head propeller turbines and returns to the ocean. EPRI reports that modified Kaplan-Turbines are used with permanent magnet generators to generate electricity [30]. In the case of extreme weather the water will simply wash over the platform harmlessly once the reservoir is full. The front of the device will have catenary anchored leg mooring and the rear a single mooring to allow the device to always turn into the wave direction. [29]

The Wave Dragon is the largest wave energy converter design today. Each unit will have a rated capacity between 4 and 11 MW, or more, depending on the wave climate. Since it is so large and stable it will likely be possible for maintenance to be done onboard the device, reducing O&M costs and downtime. [29]

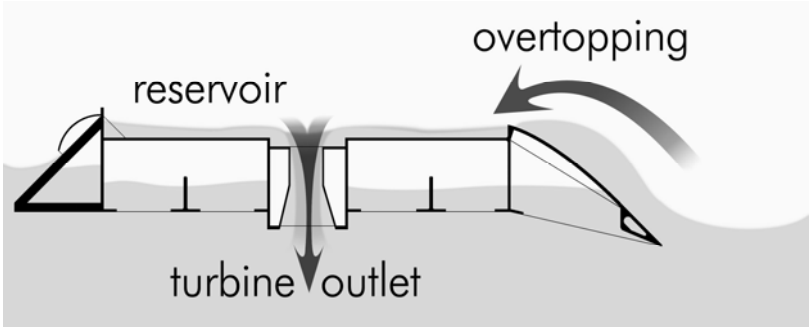

Figure 3: Wave Dragon operating principle [37]

Wave Dragon has tested a prototype rated at 20 kW in northern Denmark for over 20,000 operational hours. The prototype was deployed in March 2003 at the Danish Wave Energy Test Center in Nissum Bredning, a sheltered inland sea. The device was tested continuously until January 2005. In 2006 the modified prototype was re-deployed

to another more energetic wave site. Results of the testing outlined wave energy absorption performance, verified system performance, and led to the redesign of some components as well as improvement of almost all subsystems. [37]

In April 2006 Wave Dragon was awarded an R&D contract with the European Commission to finalize the design and construction of a multi-MW WEC. They are now in the process of developing a pilot test zone in the Irish Sea, close to Milford Haven, Pembrokeshire, Wales. They intend to deploy a 4 to 7 MW device and test it for 3-5 years to prove its commercial viability. Following initial testing, the device will be moved to a more energetic site approximately 19 km offshore. [29]

3.3 Resource Assessment

Archived wave data from the Marine Environmental Data Services (MEDS) of the Department of Fisheries and Oceans Canada was downloaded for five locations near Haida Gwaii [38]. Data for all five locations was provided by buoys operated by the Meteorological Service of Canada. The locations of these buoys can be seen in Figure 4, where the buoys are represented by teardrop shape markers. Measurements of H_s and T_p were reported hourly from January 2000 until June 2009. Only data classified as good or acceptable by MEDS was kept.

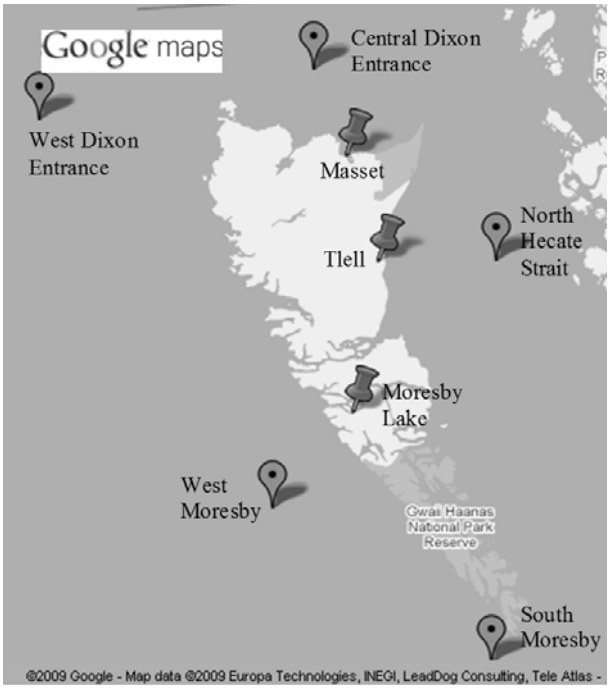

Figure 4: Wave buoy locations [41]

Theoretical wave power based on equation (8) was calculated for each buoy location. Typical years of this theoretical wave power are shown in Appendix A, where it can be seen that annual mean wave power is significantly higher for the buoys located on the west coast of Haida Gwaii. The annual mean theoretical wave power was found to be on the order of 40 kW/m for the West Dixon Entrance, South Moresby, and West Moresby locations, while it was found to be on the order of 10 kW/m for the Central Dixon Entrance and North Hecate Strait locations. These findings are supported by Andrew Cornett's Inventory of Canada's Marine Renewable Energy Resources [4].

Following this, buoy data was sorted according to month, day, hour and year, and classified by month. A coverage value was calculated for each month as many months had hours of missing data; this was done using a method adopted from Dunnett [39]. This coverage value, ζ, represents the percentage of available data in each month,

$$\varsigma_{loc,m,y} = \frac{h_{loc,m,y}}{d_{m,y}24}, \tag{9}$$

where h represents the total hours of available buoy data at a given location and $d_{m,y}$ represents the number of days in month m and year y. Months with coverage values below 90% were excluded from the analysis, while hourly wave power was calculated for the rest.

To convert hourly wave data to output power from each WEC, device performance data reported by the manufacturer was found for all three converters discussed in the previous section. Performance data for the AquaBuOY (Table 2), sized at 250 kW capacity, is reported to have been calculated based on a frequency domain numerical model of the device, where power values represent the upper theoretical fluid power available [40]. According to Pelamis Wave Power, specifications for the Pelamis device (Table 3), sized at 750 kW, were derived using an experimentally verified numerical model [35] that assumed a two parameter Pierson-Moskowitz spectra as input and took into account design constraints and machine efficiency. Period was presented in the form of T_{pow} and it was assumed that $T_{pow} = T_e$ [39] and $T_p = \alpha T_e$, where the value $\alpha = 0.9$ was chosen for this study [4]. Little is known of the derivation of the Wave Dragon performance data for a 7 MW capacity unit reported by Dunnett (Table 4 [39]). It is

likely that performance data originates from numerical model output validated by prototype sea trials since the Wave Dragon prototype has been tested extensively.

Power was calculated for measurements of H_s and T_p by interpolating between given values in the performance data tables. Dunnett [39] recommends that one interpolate between values in the performance data rather than round to the nearest value to minimize error in the analysis. No downtime for repairs and maintenance was included in the analysis.

Table 2: AquaBuOY output power for varying sea states (kW) [40]

	Tp [s]									
Hs [m]	6	7	8	9	10	11	12	13	14	17
1.0	6	8	11	12	11	10	8	7		
1.5	13	17	25	27	26	23	19	15	12	7
2.0	24	30	44	49	47	41	34	28	23	12
2.5	37	47	69	77	73	64	54	43	36	19
3.0	54	68	99	111	106	92	77	63	51	27
3.5		93	135	152	144	126	105	86	70	38
4.0		122	176	198	188	164	137	112	91	49
4.5			223	250	239	208	173	142	115	62
5.0			250	250	250	250	214	175	142	77
5.5			250	250	250	250	250	211	172	92

Table 3: Pelamis output power for varying sea states (kW) [35]

	Tp [s]															
Hs [m]	5.6	6.1	6.7	7.2	7.8	8.3	8.9	9.4	10.0	10.6	11.1	11.7	12.2	12.8	13.3	13.9	14.4
1.0	0	22	29	34	37	38	38	37	35	32	29	26	23	21			
1.5	32	50	65	76	83	86	86	83	78	72	65	59	53	47	42	37	33
2.0	57	88	115	136	148	153	152	147	138	127	116	104	93	83	74	66	59
2.5	89	138	180	212	231	238	238	230	216	199	181	163	146	130	116	103	92
3.0	129	198	260	305	332	340	332	315	292	266	240	219	210	188	167	149	132
3.5		270	354	415	438	440	424	404	377	362	326	292	260	230	215	202	180
4.0			465	502	540	546	530	499	475	429	384	366	339	301	267	237	213
4.5			544	635	642	648	628	590	562	528	473	432	382	356	338	300	266
5.0				739	726	731	707	687	670	607	557	521	472	417	369	348	328
5.5				750	750	750	750	750	737	667	658	586	530	496	446	395	355
6.0					750	750	750	750	750	750	711	633	619	558	512	470	415
6.5					750	750	750	750	750	750	750	743	658	621	579	512	481
7.0						750	750	750	750	750	750	750	750	676	613	584	525
7.5							750	750	750	750	750	750	750	750	686	622	593
8.0								750	750	750	750	750	750	750	750	690	625

Table 4: Wave Dragon output power for varying sea states (kW) [39]

	Tp [s]												
Hs [m]	5	6	7	8	9	10	11	12	13	14	15	16	17
1.0	150	250	360	360	360	360	360	360	320	280	250	220	180
2.0	640	700	840	900	1190	1190	1190	1190	1070	950	830	710	590
3.0		1450	1610	1750	2000	2620	2620	2620	2360	2100	1840	1570	1310
4.0			2840	3220	3710	4200	5320	5320	4430	3930	3440	2950	2460
5.0				4610	5320	6020	7000	7000	6790	6090	5250	3950	3300
6.0					6720	7000	7000	7000	7000	7000	6860	5110	4200
7.0						7000	7000	7000	7000	7000	7000	6650	5740

Potential locations for a WEC device were assessed based on their average annual capacity factor (CF) and relative proximity to the existing grid. CF is defined as the total output energy from a device over a period of time divided by the potential output energy if the device had been operating at full capacity the entire time. This represents average expected output energy for each device with respect to each unit of capacity installed, and is important considering the high capital cost of devices. A high CF reduces the number of devices required to reach a certain level of energy output, therefore resulting in a lower capital cost. Hourly output wave power was used to determine monthly CF for each device at each location for all years of data. From this the average monthly CF was determined for each device at each site, leading to an average annual CF (Table 5), with the highest capacity factors seen at the South Moresby, West Moresby, and West Dixon Entrance locations. Additionally, the highest capacity factors were seen with the Wave Dragon device.

An analysis of the distance from the buoy location to shore, as well as the distance on shore to the nearest grid connection point, was done via Google Maps [41]. It can be seen that the distance for the West Dixon Entrance and South Moresby locations are significantly larger than the other locations. Note that it was assumed that no over land transmission lines would be allowed in the Gwaii Haanas National Park Reserve.

The West Moresby location appears to be an interesting option as the distance to the grid is much smaller and it also has a high CF. It is likely that other locations along the west coast of Moresby Island closer to the Moresby Lake Hydro facility, where power can be transmitted to the grid, have a similar wave climate. Therefore, the transmission distance could be even less than stated. Although the CF for the Central Dixon Entrance

location is relatively low, it is located close to a major load center, Masset, which gives it the potential to also be a viable option.

Table 5: Wave energy potential by location

Buoy Location	Average Annual CF			Distance to shore (km)	Distance on land to grid (km)	Total Distance (km)
	AquaBuOY	Pelamis	Wave Dragon			
West Dixon Entrance	27%	25%	29%	80	60	140
Central Dixon Entrance	10%	10%	12%	40	3	43
North Hecate Strait	10%	9%	10%	50	1	51
South Moresby	30%	28%	32%	120	20	140
West Moresby	28%	26%	31%	45	17	62

Additionally, the hour-to-hour change in output power for each device was analyzed. It is desirable to have small hourly fluctuations in order to improve ease of system integration. To compare all devices equally, the output power was normalized according to the device's capacity. This gave a percentage change for each hour with respect to total installed capacity. The average hour-to-hour output change was calculated for each month for all years of data, and a monthly site average was calculated from all of those results. The average hourly output power fluctuation for each device at the West Moresby location is shown in Table 6. The months of January, April, August and October are shown to represent the varying seasons. Results indicate that average hourly fluctuations are less than 10%, with the largest hourly fluctuations usually seen in the AquaBuOY WEC. The same pattern is seen in the other buoy locations as well.

Table 6: Average hour-to-hour wave power output fluctuation, West Moresby location

Month	Device		
	AquaBuOY	Pelamis	Wave Dragon
Jan	9.4%	8.0%	8.3%
Apr	5.2%	4.8%	4.8%
Aug	1.7%	1.8%	1.4%
Oct	7.2%	6.5%	6.8%

Chapter 4

Modeling the Haida Gwaii Network

In order to predict the impact of integrating intermittent tidal and wave power into the Haida Gwaii generation system, an energy system model was built. This chapter outlines the existing network and the mixed integer optimization model that was built to simulate the network, including model parameterizations and input data.

4.1 Existing Network

Haida Gwaii is an archipelago made up of approximately 150 islands off the northwest coast of British Columbia (BC), Canada. Dominated by two main islands, Graham to the north and Moresby to the south, Haida Gwaii stretches for approximately 300 km. According to the 2006 Statistics Canada census, the population of Haida Gwaii was 5063 [2] with the majority of the population living on Graham Island in the towns of Masset, Old Masset, Port Clements, Tlell, Skidegate and Queen Charlotte City, and on Moresby Island in the community of Sandspit.

The two independent generation distribution systems on Haida Gwaii are referred to as North and South and are only 10 km apart at their nearest point [2]. The north system, or grid, serves approximately 1400 customers in the towns of Masset, Old Masset, and Port Clements, and the south grid serves 1600 customers in Tlell, Skidegate, Queen Charlotte City and Sandspit [2]. Each customer can represent a household or more than one person. The north grid is powered solely by Masset Diesel Generation Station (DGS) which has a capacity of 11.4 MW and is composed of 7 separate generation units of varying size [3, 22]. Its peak load and total generation in 2005 were 4.8 MW and 25.5 GWh respectively [3, 22]. The south grid is powered primarily by an independent power producer (IPP) hydro electric power plant with a capacity of 5.7 MW [2, 22]. This facility, owned and operated by EPCOR Power L.P., uses Moresby Lake on Moresby Island as its reservoir. There is also a BC Hydro owned backup diesel generation system at Sandspit with a capacity of 9.15 MW, composed of 7 separate generation units of varying size [3, 22]. In 2005, the peak load of the south grid was 5.6 MW with BC Hydro generating a total of 8.2 GWh from Sandspit DGS and buying 18.2 GWh, equal to 70% of annual demand, from the IPP [3, 22].

Figure 5 shows the geographical layout of the generation systems. Individual generation units at each DGS are detailed in Table 7. Transmission of electricity is generally done via 25 kV 3-phase transmission lines; however, there are several exceptions including the submarine cable linking Graham Island to Moresby Island via Skidegate Inlet and the IPP owned 69 kV line linking the Moresby Lake hydro facility to the southern grid [3]. Transmission line details are provided in Table 8 below. Note that the transmission system is simplified for this analysis.

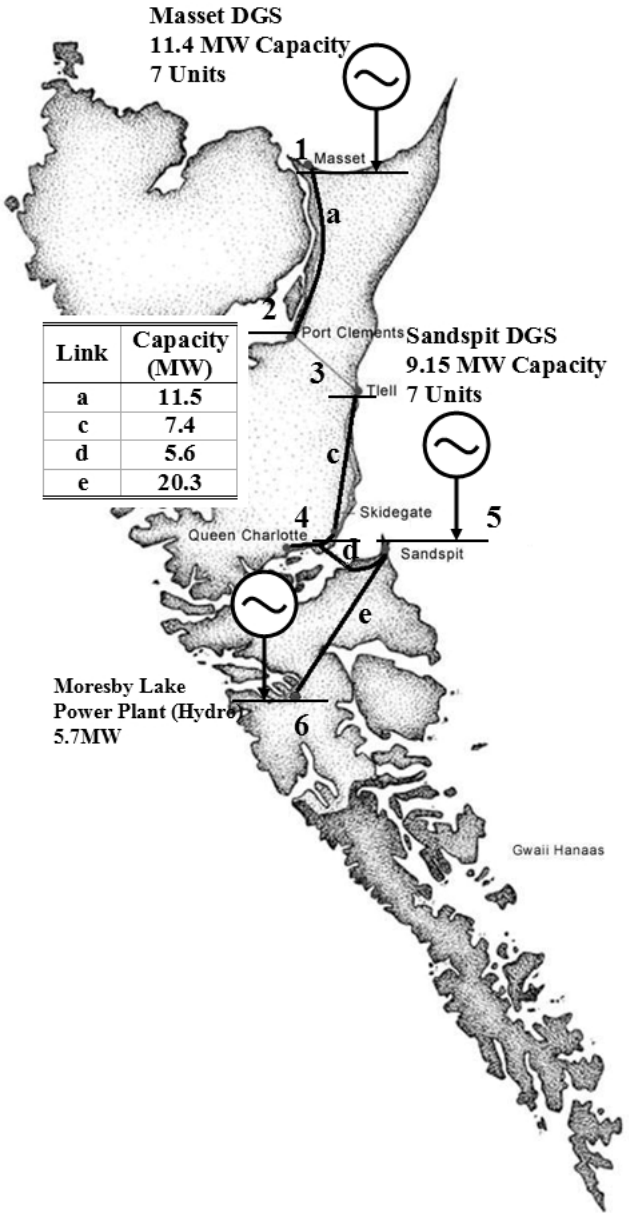

Figure 5: Haida Gwaii electricity system (data from [3])

Table 7: Diesel generating units in Haida Gwaii [3]

Masset DGS		Sandspit DGS	
Unit	Size (kW)	Unit	Size (kW)
MASG1	2108	M124G1	2500
MASG2	2108	M178G1	1600
MASG3	2108	M167G1	850
M125G1	2500	SPTG1	1600
M172G1	850	SPTG2	1600
M174G1	850	SPTG3	1000
M165	1000	SPTG4	1000

Table 8: Haida Gwaii transmission line information (data from [3])

Link Assigned Label	Bus connections	Voltage (kV)	Length (km)	Resistance [43] (Ohms/km)	Current Carrying Capacity [44] (A)	Notes
a	1-2	25	50	0.1688	460	3 phase, 336.4 kcmil conductor size, ASC type
c	3-4	25	40	0.3368	295	3/0 AWG, single phase, ASC
d	4-5	25	5	0.5351	225	1/0 AWG submarine cable
e	5-6	69	49	0.3368	295	3/0 AWG, single phase, ASC*

* Assumed line type

4.2 Network Optimization Model

To study the economic and technical implications of integrating tidal power and linking the two grids, a network model that minimizes cost subject to a set of constraints was constructed. The model consists of six buses representing transmission substations with five links connecting them. The north grid is represented by bus 1 and 2, where 1 represents the town of Masset and 2 Port Clements. For the south grid, bus 3 represents Tlell, bus 4 Skidegate and Queen Charlotte City, bus 5 Sandspit, and bus 6 Moresby Lake hydro facility. Each bus can include power contributions from generators and other buses, as well as power leaving for other buses and local demand. Note that bus 1 includes a sink where energy can be dumped as needed and any of these variables can be

zero at any time. In the event that the grids are not linked, a sink was also placed at bus 6. Links that currently exist are drawn with a solid line, whereas proposed link b is drawn with a hatched line.

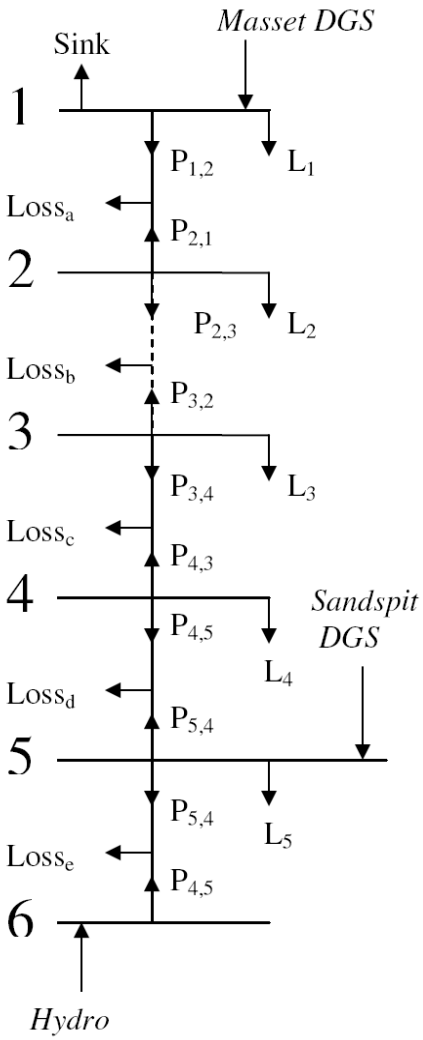

Figure 6: Network Diagram

The power at each bus at any time, *t,* must balance. This results in a bus power balance:

$$\sum_{n} P_{i,n,t} + L_{i,t} + sink_{i,t} - G_{i,t} = 0 \forall i = 1,2,...,I \;\&\; t = 1,2,...,T\,, \tag{10}$$

where $P_{i,n,,t}$ represents the power transferred from bus i to bus n at time t. $L_{i,t}$ and $G_{i,t}$ represent the load and total energy generation at bus i and time t. Applying this to the

above network gives six equations, one for each bus, which are used as constraints in the model. Note the non-negativity of load, energy generated, and energy sent to the sink,

$$L_{i,t},\ G_{i,t},\ sink_{i,t} \geq 0 \forall i = 1,2,...,I \ \& \ t = 1,2,...,T, \tag{11}$$

Transmission line constraints include line losses and current carrying capacity. Since power leaving a bus is defined as positive, power is entering the link from opposite directions. Figure 7 below shows the power balance on each link. This results in one of the power terms being negative. Furthermore, one of the power terms must be smaller than the other to make up for the transmission losses which are determined from the following equation,

$$Loss_{j,t} = \frac{\max(P_{i,n,t}{}^2, P_{n,i,t}{}^2) R_j}{V_j^2} \forall j = 1,2,...,N \ \& \ t = 1,2,...,T, \tag{12}$$

where R_j and V_j represent the resistance and voltage of link j, and N represents the total number of links. The current on each line is constrained so that the maximum allowable current, or current carrying capacity, is not exceeded. Table 8 outlines the reported voltages, lengths, and type of each existing line. Resistances and current carrying capacity were estimated from the type of line [43, 44]. The link from bus 2 to 3 is assumed to be 20 km in length, 25 kV, 3/0 AWG, single phase, ASC type, where length and voltage were estimated based on the Haida Gwaii Community Electricity Plan released in April 2008 [2].

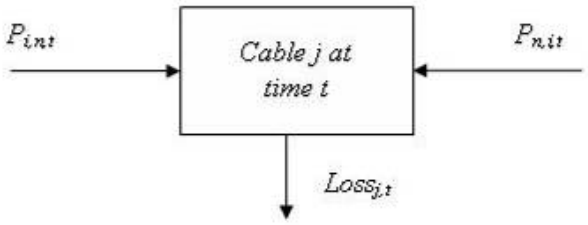

Figure 7: Power Balance of the link between bus i and n (modified from [42])

Multiple constraints exist due to the nature of each generator. For dispatchable generators, where output can be increased or decreased as desired, generation cannot exceed capacity

$$G_{d,t} \leq G_{d,cap} \forall d = 1,2,...,D \ \& \ t = 1,2,...,T, \tag{13}$$

where $G_{d,t}$ is output from dispatchable generator d at time t and $G_{d,cap}$ is the capacity of generator d. Generators must also stay within ramping rate limits dependent on the type of generator. Diesel generators in the Haida Gwaii network are capable of ramping up to their full capacity from zero output within the one-hour time step used in this model [45]. Similarly, ramping down can be done within a period of one hour, indicating that ramping rate constraints are, in fact, not needed in this case. BC Hydro's preference is to operate all diesel generation units at a minimum output level of 50% part load [3, 22]. For example, this means that a 1 MW unit can operate at a minimum level of 0.5 MW while on. This led to the inclusion of a binary variable, $x_{d,t,}$, that indicates whether a unit is operating during a specific time period, where $x_{d,t,}$ is equal to 1 if the unit is on and 0 if the unit is off.

In reality, hydro power generation is limited by reservoir volume. Unfortunately temporal data on reservoir volume were unavailable; however, actual hourly power generated in 2006 from the hydro facility was available [3]. Therefore, hourly generation from the hydro facility was used as a direct input to the model and assumed must-take to match the current operating strategy [3].

Operating costs have been assigned to each diesel generating unit at Masset and Sandspit DGS. The fuel costs of the diesel generating units were determined from industry-reported fuel consumption values (gal/hr) as a function of part load [46] and a cost of 1$/L for diesel fuel [22]. A second order polynomial curve was fit to the data for each size of generator and plotted in a total production cost curve (Figure 8). The cost of operating each unit at the minimum operational level of 50% part load was determined from the total production cost curve. The incremental cost of increasing the output power another unit was determined by calculating the slope of the total production curve at 10 different power levels (Figure 9). This approach is taken from Muckstadt [13] and allows the objective function to be linear, thereby greatly reducing the computational complexity. The number of cost levels for each generator is represented by K_d and in this case is set at 10 for all generators. The incremental generation for each cost level is represented by $M_{d,k}$. In Figure 9, $M_{d,k}$ is equal to 0.05 MW for all cost levels, or 5% of the total generator capacity. Incremental generation levels were kept at 5% of total generator capacity for all generators.

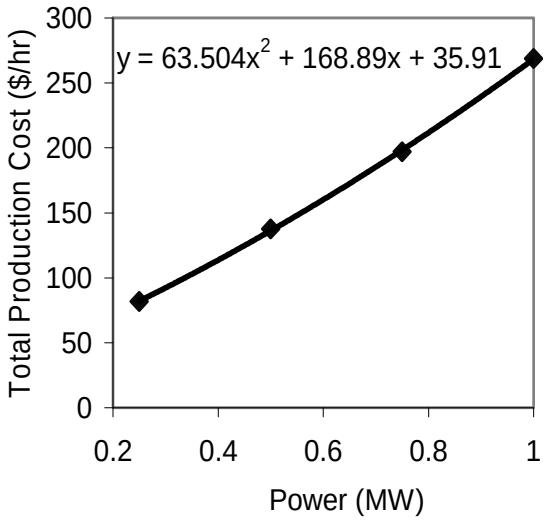

Figure 8: Total production cost curve for a 1 MW capacity diesel generator

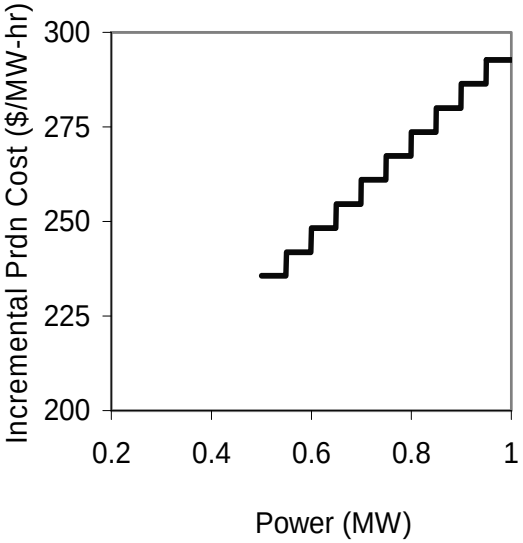

Figure 9: Incremental production cost curve for a 1 MW capacity diesel generator

Costs were also applied to maintenance and cycling of diesel generators. The cost associated with maintenance for the diesel generation units, c_{maint}, was calculated based on an overhaul life estimate of 30,000 hours in operation and overhaul cost of $200,000, resulting in a cost of $6.67 per hour in operation [45]. Cycling of diesel generators leads to an increased rate of degradation of the unit over time [47]. As a result, operators avoid constantly shutting down and starting up units. To mimic this behaviour, a cost was applied to the action of starting up and shutting down a generator where $c_{su,d}$ is the start-up cost and $c_{sd,d,}$ is the shut-down cost of generator d.

The objective of the model is to minimize total system operating cost subject to the constraints outlined in equations (10), (11), (12) and those shown below in equations (15) through (20). Note that equation (13) is implicit in the objective function. The problem statement, modified from [13], is as follows:

$$\min \sum_{t}^{T} \sum_{d}^{gens} \left[c_{su,d} w_{d,t} + c_{sd,d} z_d + h_t c_{min,d} x_{d,t} + \sum_{k}^{K} M_{d,k} h_t g_{d,k} y_{d,k,t} + c_{maint} x_{d,t} \right] \quad (14)$$

s.t.

$$0 \le y_{d,k,t} \le x_{d,t} \quad (15)$$

$$w_{d,t} \ge x_{d,t} - x_{d,t-1} \quad (16)$$

$$z_{d,t} \ge x_{d,t-1} - x_{d,t} \quad (17)$$

$$w_{d,t}, z_{d,t} \ge 0 \quad (18)$$

$$x_{d,t} \equiv binary \tag{19}$$

$$\left|P_{i,n,t}\right| \leq LineCapacity\,, \tag{20}$$

where $c_{min,d}$ is the cost in dollars of operating generator d at its minimum capacity for 1 hour, h_t is the number of hours in period t, $g_{d,k}$ is the incremental production cost of operating generator d at cost level k, and $y_{d,k,t}$ is the percent of available capacity, $M_{d,k}$, that is used in period t. Equation (15) illustrates that $y_{d,k,t}$ can only be greater than zero if $x_{d,t}$ is 1, indicating that the unit is on. It can also be seen from equation (16) that $w_{d,t}$ equals 1 if unit d is started in period t and zero otherwise. Likewise, equation (17) shows that $z_{d,t}$ equals 1 if unit d is shut down in period t and zero otherwise. Equation (20) indicates that the power along a line cannot exceed the capacity of that line determined from rated voltage and current carrying capacity.

Since both hydro and tidal power are considered non-dispatchable in the model, costs associated with them were not optimized. Rather, fixed costs associated with hydro and tidal power can be added to the optimized solution to find the total system cost.

Total carbon dioxide emissions were calculated for each case based on fuel consumption of the diesel generators and 10.1kg CO_2/gal(US) of diesel fuel [48] such that

$$\mathrm{E}=\sum_{t}^{T}\sum_{d}^{gen} e_{d,t} G_{d,t}\,, \tag{21}$$

where E is total CO_2 emissions in time period T and $e_{d,t}$ is kg CO_2 per MWh for generator d at time t. To find $e_{d,t}$, industry-reported diesel fuel consumption data (gal/hr) as a function of output [46] was converted to kg CO_2/MWh and a quadratic equation was fit to the data (Figure 10).

The model was built using a Matlab (The MathWorks Inc.)/General Algebraic Modeling System (GAMS Development Corp.) environment, where data was input into Matlab and GAMS solved the optimization through a call from Matlab. GAMS solved the problem with the Cplex solver, which utilizes a branch and cut algorithm to solve a series of linear subproblems and converge on a solution for the mixed integer linear program [49].

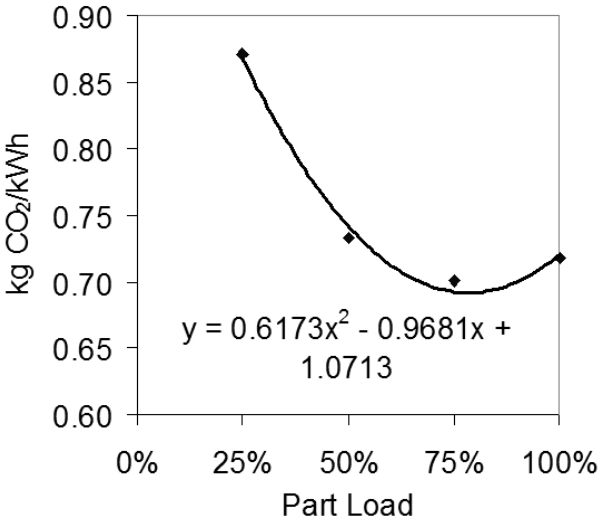

Figure 10: Diesel generator emissions for a 1 MW capacity unit

4.3 Model Parameterization

To more accurately model generation for both grids in Haida Gwaii, adjustments were made to the model. Three generation units at Masset DGS and three at Sandspit DGS were reported to be in undependable condition [22]. These units included MASG1, MASG2, MASG3, M178G1, SPTG4, and SPTG5, all of which are 21-30 years old and were identified as having mechanical problems. Therefore, these units were removed from the model.

It was found from initial model results that transmission losses along each link were at maximum 1% of the power being transferred. Therefore, it was assumed that these losses were negligible and the constraints in the model representing transmission line loss were removed in order to reduce computational time. Current carrying capacity constraints were not removed, and power flowing along each link was still accounted for. The only change was that losses were assumed zero.

Costs for the non-optimized hydro and renewable energy were included in the analysis post-optimization. A cost of $0.061/kWh was used for the power provided by EPCOR from the Moresby Lake hydro facility, which was the average IPP purchase price by BC Hydro in 2008 [50]. Since tidal and wave power are not yet in the commercial phase, a reasonable operation and maintenance (O&M) cost was unknown. Rather than

speculating on a cost, no O&M cost was included and the maximum economically viable cost for the project was determined, which includes the project's O&M costs.

Since the actual cost of starting-up or shutting down a unit can not easily be determined, and estimates for these costs vary widely [45, 47], it was decided to keep the values of $c_{su,d}$ and $c_{sd,d}$, low to mimic the behaviour of reduced cycling while not affecting overall cost. A sensitivity study was done for the linked grids case (Figure 11) as well as the separate north and south grids case. A value of $200 was chosen for both $c_{su,d}$ and $c_{sd,d}$ as it reduced the number of start-ups by 50% while only increasing the total operational cost of the system by 2%.

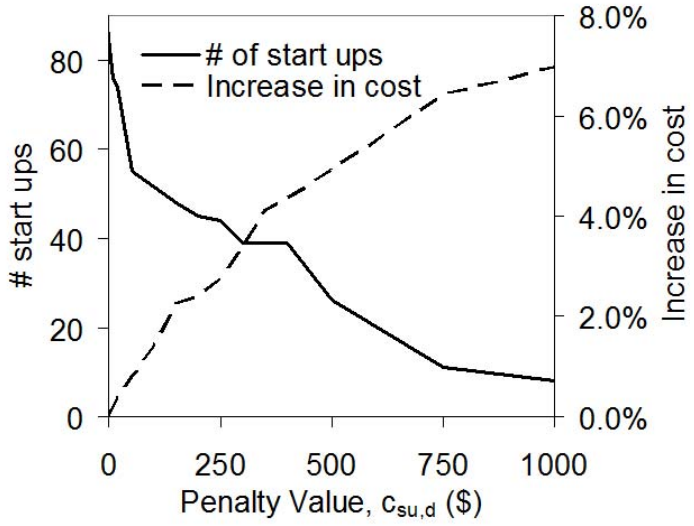

Figure 11: Sensitivity results for linked grids case, month of January data

The model was validated through several means. It was tested with multiple simple cases to confirm that it provided the least cost solution and no constraints were violated. Furthermore, the problem was solved with three different solvers including Cplex, Coincbc and Coinglpk, all of which provided the same solution.

4.4 Model Input Data

4.4.1 Load Data

Load data was supplied by BC Hydro. For the south grid, hourly generation data for both the IPP facility and Sandspit DGS were provided for 2007. It was assumed that the combination of these two generation loads at each hour was equal to the south grid's

demand. For the north grid, actual hourly load data was not available; rather, the maximum and minimum demand day in a given month was provided for 2005 (Figure 12). To manufacture daily load data for the north, a distribution profile of data for each hour was needed.

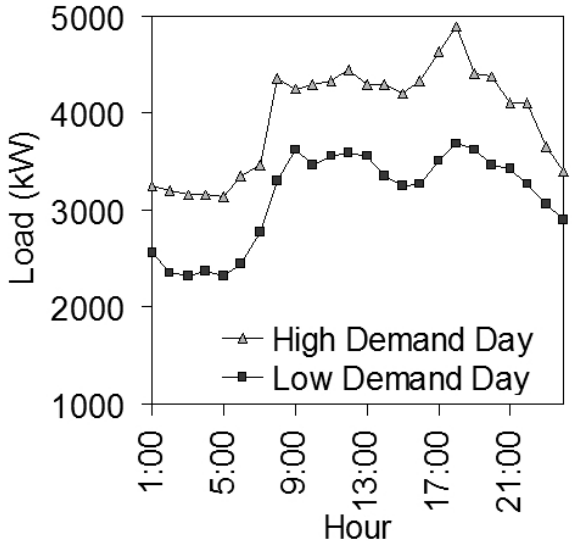

Figure 12: Masset DGS Jan-05 maximum and minimum load [3]

Since the only extensive data available were from the south grid, load data categorized by hour for each month from the south grid were analysed with a Lilliefors test and found to follow a normal distribution 82% of the time at a significance level of 1%. Each hour in the months of January, April, August and October was analyzed, resulting in 96 different test results. The Lilliefors test, similar to the Kolmogorov–Smirnov test, uses the test statistic

$$KS = \max \left| SCDF(x) - CDF(x) \right|, \tag{22}$$

where *SCDF* is the empirical cumulative distribution function (CDF) estimated from the sample and *CDF* is the normal CDF with mean and standard deviation equal to the mean and standard deviation of the sample [51]. The data were also tested for other distributions and were found to fit the normal distribution the best. The load for each hour in a given month in the north grid was assumed to follow a normal distribution similar to that of the south. Based on this assumption, multiple days of data were randomly generated for each month, resulting in a year of hourly north load data.

Another problem arose in that load is distributed throughout the grid, but only total load for each grid was known. Therefore, load at each bus was calculated based on the population at each bus:

$$L_i = \left[\frac{pop_i}{pop_{tot}} \right] L_{tot}, \tag{23}$$

where L_i represents load at bus *i*, pop_i represents the population at bus *i*, pop_{tot} represents the total population of the grid in which bus *i* is located, and L_{tot} represents the total load of that grid. Individual community populations were provided by the 2006 Statistics Canada census [2].

4.4.2 Tidal Power Data

Hourly tidal power data for Masset Sound was calculated for an entire year using the model developed by Blanchfield [27]. Turbine drag factors varying from 0.001 to 0.046 at increments of 0.001 were used, resulting in 46 different levels of tidal input. This corresponded to a maximum of 0.22 to 9.85 MW of tidal power available in a given hour. It is assumed that the maximum tidal power available is equal to the installed tidal capacity. *Tidal power penetration* is the level of installed capacity over peak demand. Given that the maximum load was 4.79 MW for the north grid and 9.85 MW for both grids combined, this represents maximum power penetration levels of 206% for the north grid alone and 100% for the linked grid case.

Another way of evaluating the level of tidal input is the ratio of total tidal energy produced to the total energy demand, often referred to as *energy penetration*. In the case of the linked grid system this level increases from 1% to 55%, and for the non-linked system it ranges from 3% to130%. This level of input in the north grid, although much higher than what is realistically expected, is informative as it allows direct comparison between the two options; however, if installed, excess power could be used for residential heating or stored for later use.

4.4.3 Wave Power Data

Two locations were considered for a wave power plant: Central Dixon Entrance (CD) and West Moresby (WM). Although CD has a low annual capacity factor, its location relative to a major load center, Masset, potentially makes it a more viable option. The WM location was more promising, with an annual capacity factor of 26-31%

depending on the device used, although farther from major load centers. The Pelamis device was selected as it is the most advanced device having undergone significant sea trials as mentioned before. Installed capacity ranged from one to thirteen devices, each sized at 750 kW. This corresponds to a maximum installation of 9.75 MW, or a maximum power penetration of 99% and 204% for the linked and non-linked grid cases, respectively.

Hourly wave power from the Pelamis WEC was manufactured for all years of available data using the technique described in Section 3.3. Each month was analysed and an individual year was selected that had a monthly CF closest to the average monthly CF for that site. This meant that data from different years were used for each month. The average annual energy penetration with 13 Pelamis devices installed for the CD location is 14% for the linked grid and 34% for the non-linked grid. The same values for the WM location are 37% and 86%, reflecting the higher CF available at the WM location.

Chapter 5

Optimization Results

The following chapter discusses the results from the optimization model. First, the effect of linking the grids is analyzed. Second, integrating tidal power from Masset sound is considered, and, third, integrating wave power from both the CD and WM locations is reviewed. To do this, the models were initially run with no renewable energy input, followed by incremental levels of renewable capacity installed. Tidal energy was assumed to be input directly into the Masset bus, as was wave energy from the CD location. This meant that when the grids were not linked, renewable energy contributed to the north grid alone. However, wave energy from the WM location was input into the Moresby Lake bus, thereby contributing solely to the south grid when the grids were not linked.

To represent variation among seasons, four separate two week time periods were modeled. These two week periods were selected from January, April, August and October. Annual results presented below are based on an average of the four time periods analyzed.

5.1 Linking the Grids

One of the immediate concerns with linking the grids is the resulting effect on system operation. The duty cycle of each generating unit, defined as the percent of time in operation, was determined when the grids were both linked and not linked (Figure 13). Linking the grids appears to reduce the number of generating units required. This can be seen in Figure 13, where duty cycles for two of the units, M174G1 and M165G1, are zero for the linked case. Conversely, the non-linked case requires all generators to operate at some point, and in all but one case the generators are used more often. An example of this is M172G1, the 0.85 MW capacity unit in Masset, which has a duty cycle of 75% when the grids are separate and 14% when they are linked. The exception to this rule is M124G1, the 2.5 MW capacity unit in Sandspit, whose duty cycle increases from 10% when the grids are not linked to 97% when they are linked. These results indicate that linking the grids would lead to heavy use of the 2.5 MW units and very light use of the other smaller units.

Furthermore, fewer start-ups and shut-downs are required for the linked case than the non-linked case. The average number of cycles, where a cycle represents a generator turning on and off, over a two week period for each generator was 5 or less for the linked case and 7 for the non-linked case (Figure 14). In fact, the number of cycles for most generators is well below BC Hydro's operational policy of cycling each generator no more than once a day [3, 22], or a maximum of 14 cycles for each generator for the two week period.

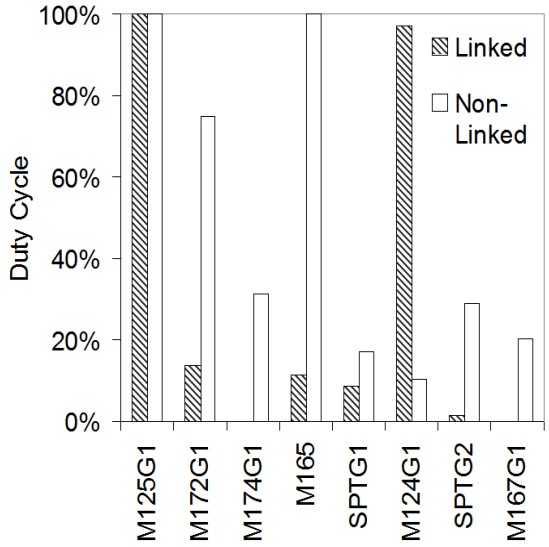

Figure 13: Diesel generator duty cycle, no renewable power

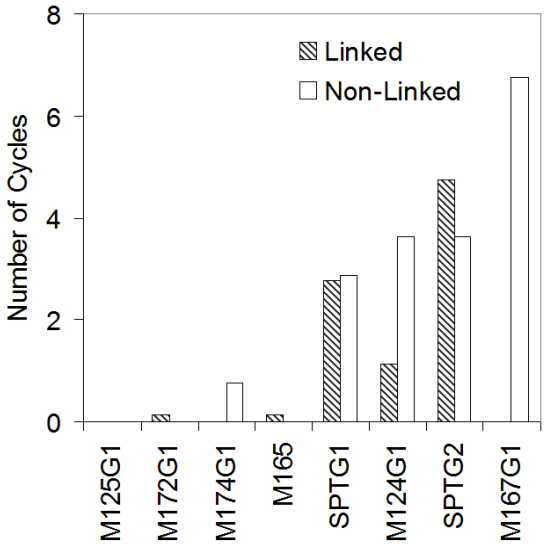

Figure 14: Average number of diesel generator cycles, no renewable power

Less than 1% of the energy produced was sent to the sink in all cases analyzed. This excess energy is due to the minimum operational level constraints placed on the generators, as well as the decision to run a larger unit than is required, and dump excess energy, rather than shut the unit down for a short period of time. Energy sent to the sink is always higher for the non-linked grid than the linked one.

The average power sent along proposed line b (Figure 6) was 1.1MW. Although power travels in both directions, it traveled most often in the south to north direction, indicating that power was being transferred from the south to the north grid. This is largely due to the extra power generated by M124G1, which is sent to the north grid and makes M174G1 in Masset redundant (shown in Figure 13).

The only line that reached its carrying capacity, and therefore limited generator operation, was line d, the underwater cable linking Graham and Moresby Islands. This capacity was reached only when the grids were linked. Most of the population, and therefore also the energy demand, is located on Graham Island [2]. Figure 13 illustrates that when the grids are linked the optimal solution is to reduce generation from Masset DGS and increase output from Sandspit DGS. This increase in power from Sandspit DGS must be sent along line d in order to be delivered to the main load center. In the non-linked grids case, the south grid load never exceeded the carrying capacity of line d, so it was a non-issue. However, in the linked grids case, the low carrying capacity of line d acted as a bottleneck in the network and restricted how much power could be sent from Sandspit DGS and Moresby Lake Hydro Facility to the north grid.

Carbon dioxide emissions were reduced only slightly for the linked grid over the non-linked grid. Average annual emissions were 0.435 kg/kWh for the current non-linked case and 0.434 kg/kWh for the linked case. The most notable difference in emissions was an increase in emissions during August, when hydro output is at its lowest.

The total cost of generation for each time period was determined by adding the set cost of hydro to the minimized diesel cost. To find the optimal average cost of electricity for the year, the costs of the four periods analyzed were combined and divided by the total energy consumption. This resulted in a cost of 0.194 $/kWh and 0.191 $/kWh for the non-linked and linked cases respectively. Given the average cost of electricity and total annual consumption [22], the total savings due to linking the grids in one year of operation was calculated as $178,000 CAN. Estimates for the capital cost of linking the grid range from $10-15M CAN [52].

5.2 Integrating Tidal Power

The addition of tidal power to the system increases the complexity of system operation. A typical snapshot of diesel generator output with 5 MW of tidal capacity installed is shown in Figure 15. This is from the non-linked grids case and shows only those generators in the north grid affected by the tidal addition. It can be seen that diesel generating units must cycle and ramp up and down more often to compensate for the varying tidal energy. Furthermore, decisions on when to cycle generating units become more complex when tidal power is added to the system. For example, at hour 27 the

level of tidal energy input exceeds the load; however, M174G1 continues to run. This decision is made because it is cheaper to keep the unit running at its minimum operational level and curtail tidal energy than to shut the unit down and start it up again in the following hour.

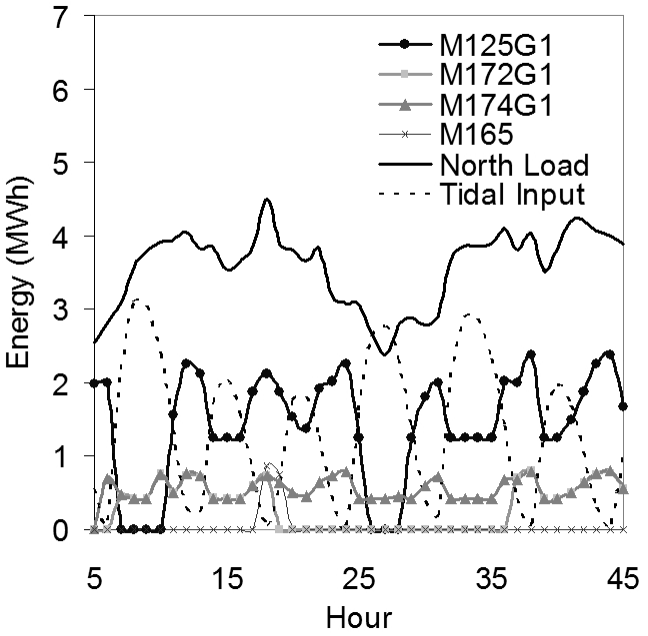

Figure 15: Typical generation, 5 MW installed tidal capacity

As installed tidal capacity increases, the duty cycle of those diesel units most often operated declines for both the linked and non-linked cases. Optimization results indicate that the largest units available should be used the most often. For the non-linked case, the only generators affected were, of course, those in the north grid (shown in Figure 16). The duty cycle for M125G1, the 2.5 MW unit in Masset, was initially at 100% with no tidal input, but declined to 56% with 5 MW of tidal capacity installed. Similarly, the duty cycle for M165, the 1 MW unit in Masset, decreased from 100% with no tidal input to 37% with 5 MW installed. It is interesting to note that the duty cycle of these two generators does not begin to decrease until installed tidal capacity reaches 2.3 MW. Rather, before 2.3 MW of tidal capacity is installed the duty cycle of the smaller diesel unit, M172G1, decreases 50%, showing that diesel generation is first replaced from the smaller generators.

Figure 17 depicts the change in duty cycle for each diesel generating unit as installed tidal capacity increases for the linked case. It was previously noted that linking the grids would eliminate the use of generators M174G1 and M167G1, and increase the use of the two 2.5 MW capacity units, M125G1 and M124G1, so that they were used far more often than the rest. When tidal power was added to the linked system M174G1 and M167G1 maintained a duty cycle of 0% until installed tidal capacity exceeded 2 MW. Likewise, M172G1, the other 0.85 MW capacity unit in Masset DGS, dropped from 14% to 0% duty cycle when tidal power was input and stayed out of use until 2.3 MW of tidal capacity was installed. Unlike the non-linked case, the duty cycle of the larger units decreased quickly as tidal capacity increased for approximately the first 5 MW of tidal capacity installed. For example, the duty cycle for M124G1 decreased 76% when 5 MW of tidal capacity was installed. It appears that initially diesel generation from the larger units is being replaced by tidal energy and generation from several smaller units. However, after approximately 5 MW of tidal capacity is installed the duty cycle for the smaller units begins to decrease and the duty cycle of the larger units levels off. This shows that there is a minimum duty cycle required for the larger units due to the cyclic nature of tidal power.

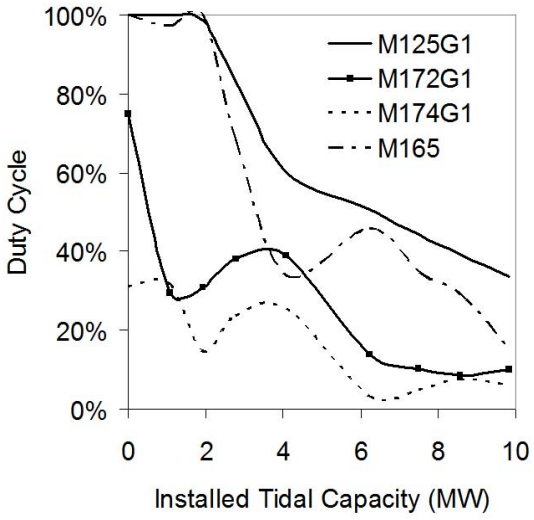

Figure 16: Diesel generator duty cycle vs. installed tidal capacity, non-linked case

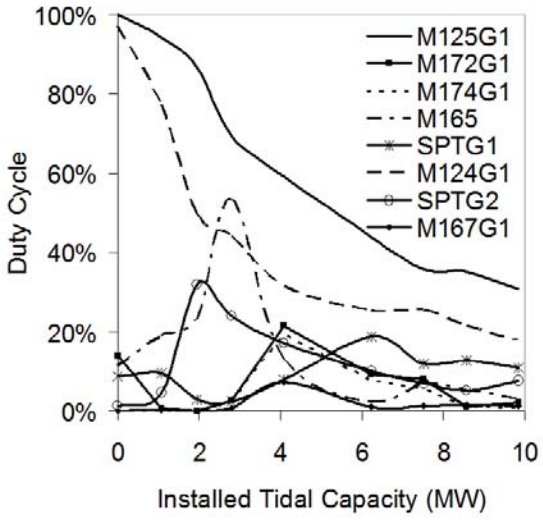

Figure 17: Diesel generator duty cycle vs. installed tidal capacity, linked case

As installed tidal capacity increased, the cyclical nature of the tidal power was amplified, resulting in an increase in the number of cycles for each diesel generating unit. The most significant increase for both the linked and non-linked cases was seen in M125G1, which reached its maximum allowable number of cycles for the non-linked case when installed tidal capacity was 2.5 MW. Likewise, M125G1 reached its maximum allowable number of cycles for the linked case when installed tidal capacity was 3.2 MW. This indicates that above these levels of installed tidal capacity the minimum cost schedule determined from optimization cannot be followed.

Average diesel generation, as well as tidal energy used and curtailed tidal energy, is shown in Figure 18 for the non-linked and linked cases with varying tidal capacity. All values have been normalized by total diesel generation from the case with no tidal energy input, which represents the total load minus the must-take hydro input. Diesel generation is always lower for the linked case than the non-linked case with the same level of tidal capacity installed, indicating tidal energy can replace more diesel generation in the linked case. Consequently, there is more curtailed tidal energy in the non-linked case. Levelling off of diesel energy generated as tidal capacity increases can also be seen, showing that increasing tidal capacity beyond a certain level provides less benefit as less diesel generation can be replaced. It also shows that excess tidal energy begins to grow quickly above 4 MW of tidal capacity installed, indicating that storage, or allowing hydro to vary, would be beneficial above this level.

The average CF of the tidal power plant, CF_{plant}, was determined as shown:

$$CF_{plant} = \frac{\sum TE_{used}}{TP_{cap}T}, \tag{24}$$

where TE_{used} represent the total tidal energy absorbed by the grid, TP_{cap} represents the tidal plant installed capacity, and T represents the total number hours in the time period analyzed. CF_{plant} is never 100% due to the cyclic nature of the tides. In fact, assuming all tidal energy produced could be absorbed by the grid, the average annual plant CF for the Masset Sound site was 39%. This represents the upper CF limit possible for the tidal plant and is henceforth referred to as the *resource CF*.

The tidal plant CF with increasing installed capacity is shown in Figure 19 for both the linked and non-linked cases. An interesting behaviour is the increase in plant CF for

the non-linked case between 2.3 and 4 MW of tidal capacity installed. This occurs because at this point tidal energy begins to replace significant amounts of diesel generation from M125G1 and M165. This can be seen in Figure 16 where the duty cycle of M125G1 drops from 95% at 2.3 MW installed to 60% at 4 MW installed. Likewise the duty cycle of M165 drops from 98% to 34% over the same period. Above 4 MW of installed tidal capacity, tidal energy cannot replace diesel generation at the same rate due to diesel generation constraints and curtailed tidal energy grows (also shown in Figure 18). This leads to the subsequent decrease in CF shown.

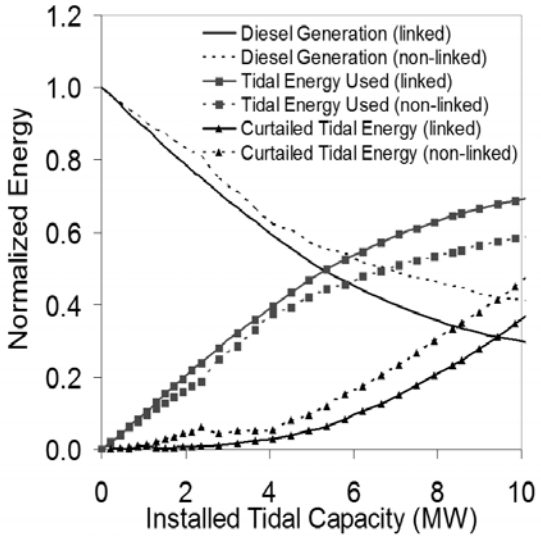

Figure 18: Energy contribution by source vs. installed tidal capacity

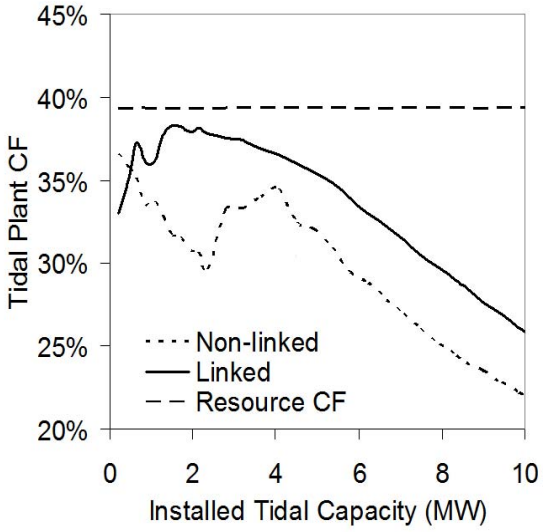

Figure 19: Optimized annual tidal plant capacity factor

Average power flowing along each line for the linked case is shown in Figure 20. In addition to the average power, the mean power on each line was found, indicating the most frequent direction of power flow. Power on proposed line b flowed primarily in the south to north grid direction until installed tidal capacity reached 5 MW, at which point power flowed from north to south grid more often. The carrying capacity of line d was reached in the linked case, leading to limits on diesel generation from Sandspit DGS. It is clear from Figure 20 that link d, which is also the most heavily constrained line, has the highest level of power flowing along it. This is also true for the non-linked case, although it never reaches its capacity when separate grids are in place. No other lines reached their carrying capacity for either the linked or non-linked cases. For the non-

linked case, power on each line was unaffected by increasing tidal capacity because the sink for excess tidal power was located in Masset, meaning any curtailed tidal power does not need to travel along any lines.

Carbon dioxide emissions for the linked and non-linked cases are shown in Figure 21. Average emissions are reduced nearly linearly from no tidal installed until approximately 4 MW is installed. This almost linear behaviour is due to a constant decrease in diesel generation with increasing tidal energy available. The slope for the linked grid emissions is slightly steeper than that of the non-linked grid, reflecting a larger decrease in diesel generation for each incremental unit of installed tidal capacity. As installed tidal capacity increases above 4 MW, the level of emissions begins to plateau due to the system's inability to continuously absorb tidal energy.

The operational cost of energy was determined from results for varying levels of installed tidal capacity. To find the operational cost of energy, the total costs for each period analyzed, consisting of optimized system cost and predetermined IPP hydro costs, were added together and divided by the total energy consumption. This was done for each level of installed tidal capacity, resulting in the curves shown in Figure 22. The cost of energy behaves very similarly to CO_2 emissions; a constant decrease is seen for both cases as installed tidal capacity increases to 4 MW, at which point cost begins to plateau, indicating diminishing returns.

Annual savings were determined for each level of tidal capacity installed by comparing total annual cost to that with no tidal capacity installed for the same grid configuration (linked or non-linked). Based on annual savings, a project life of 20 years, and a discount rate of 6%, the net present value of the project was determined and divided by installed capacity, referred to as the *break even project cost* (Figure 23). A break even cost indicates that above this cost electricity would be more expensive than if no tidal capacity were installed at all. Since operational costs of a tidal energy power plant were unknown, this maximum allowable cost includes overnight tidal plant O&M costs. Furthermore, costs associated with any transmission lines required are also included in the break even project cost. Break even costs vary slightly due to small changes in the slopes of the lines in Figure 22, which are amplified when assuming a long term project life. The break even project cost is always higher for the linked case and

low levels of installed tidal capacity, therefore making it more economical to integrate tidal power when the grids are connected and at low penetration levels. Overnight capital cost estimates from the US Energy Information Administration, in terms of 2007 US dollars, are on the order of 2000 $/kW for onshore wind, 3800 $/kW for offshore wind, 2300 $/kW for hydroelectric, and 5500 $/kW for photovoltaic [53]. These estimates do not include O&M or transmission line costs however.

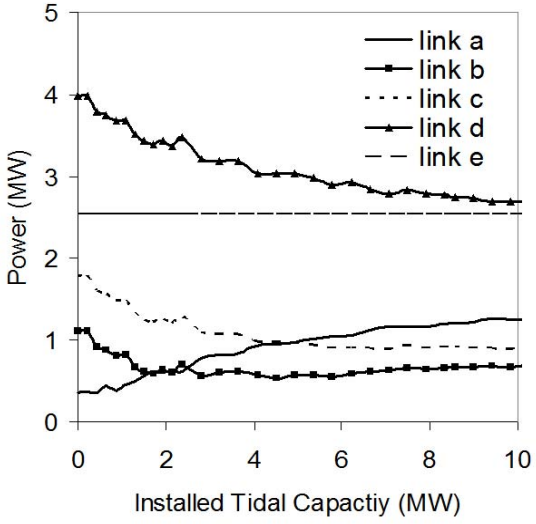

Figure 20: Average line power flow vs. installed tidal capacity, linked case

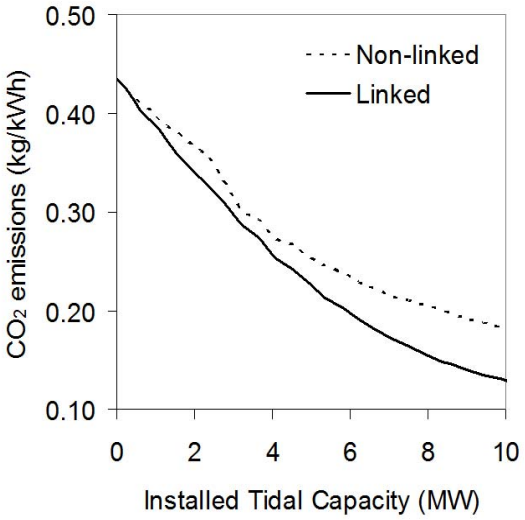

Figure 21: Average CO_2 emissions vs. installed tidal capacity

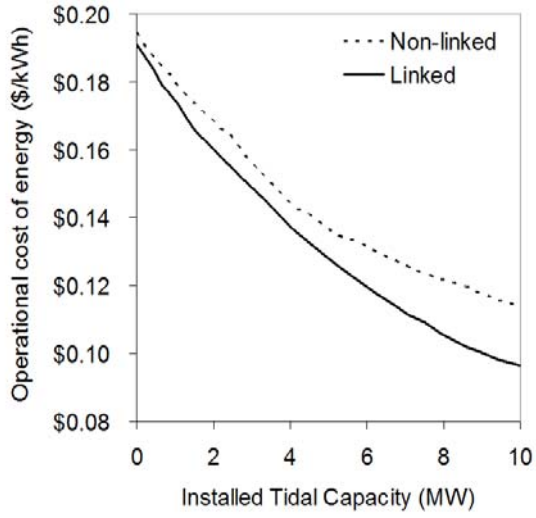

Figure 22: Annual operational cost of energy vs. installed tidal capacity

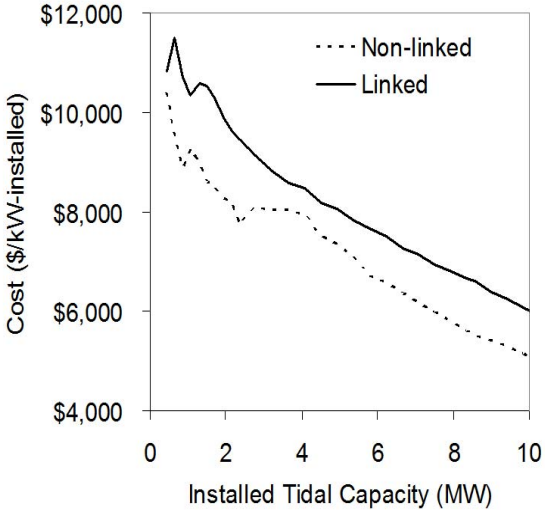

Figure 23: Break even project cost vs. installed tidal capacity

It is apparent from this analysis of the technical and economic impacts of tidal power integration into the Haida Gwaii grid that tidal power is feasible at low levels of installation. A similar analysis will now be done on the impacts of wave power integration.

5.3 Integrating Wave Power

The effects of integrating wave energy into the Haida Gwaii system are largely dependent on energy penetration levels. The average annual CF of the wave resource in the CD location for the Pelamis device was found to be 10% (Table 5). This meant that wave power input had little impact on the system at low levels of installed capacity. In fact, wave energy penetration did not reach 10% of total linked system load until installed capacity reached 6.75 MW. Figure 24 shows total diesel generation, as well as wave energy used and curtailed, normalized by total diesel generation with no renewable input. Normalized diesel generation and wave energy used represent the percent contributions of each that meet the remaining load after hydro power has been used. It can be seen that wave power does not replace significant amounts of diesel generation in the CD location for either the linked or non-linked grids case.

The WM location benefits from a higher annual wave resource CF than the CD location, namely 26% for the Pelamis device (Table 5), indicating larger effects on system operation. It can be expected that wave power would replace more diesel generation; however, in the non-linked grids case, wave power is contributing to the south grid, which already benefits from significant hydro power. This means that there is not much diesel generation to displace when the grids are not linked, especially in the winter months when hydro output is at its peak.

Figure 25 shows the normalized average diesel generation, wave energy used and wave energy curtailed as was done for the CD location in Figure 24. A significant difference between the linked and non-linked cases is seen, with far more diesel generation being replaced and wave energy being used in the linked case. As mentioned before, this is due to the abundant must-take hydro power already present in the south grid. However, wave energy is still significantly limited in the linked case as installed

capacity increases due to the carrying capacity constraint of line d, the submarine cable linking Moresby and Graham Islands. This line was found to reach its carrying capacity when the grids were linked with no renewable installed at all, limiting the power that could be generated by Sandspit DGS and the Moresby Lake Hydro Facility; therefore, it is evident that it will only become a more significant bottleneck as wave energy generation capacity is installed on Moresby Island, resulting in curtailment of wave energy from the WM location.

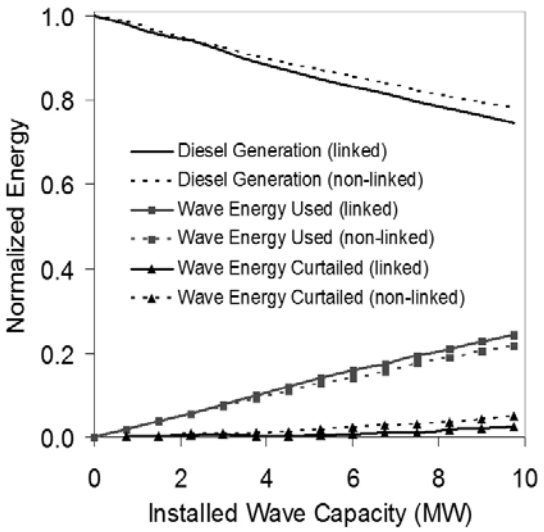

Figure 24: Energy contribution by source vs. installed wave capacity, CD location

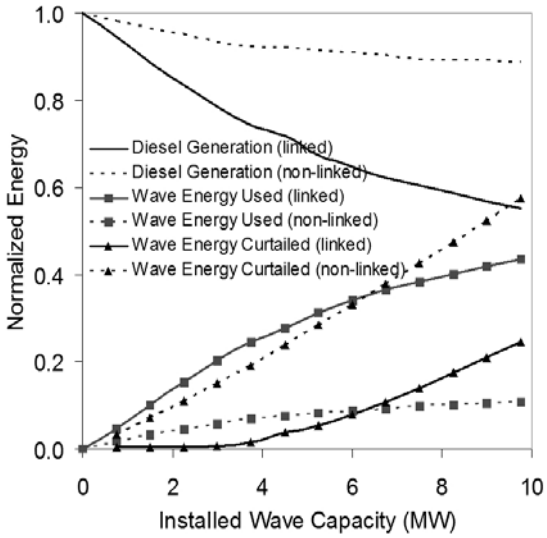

Figure 25: Energy contribution by source vs. installed wave capacity, WM location

Diesel generator duty cycle varied only slightly with increasing installed wave capacity for the CD location. This effect was seen for both the linked and non-linked grids cases (Figure 26 and Figure 27). In both cases, the larger capacity generation units were used the most often and the smaller units used less. In the linked grids case, the duty cycle of the two largest units, both sized at 2.5 MW capacity, decreased 20% and 50% with 9.75 MW of wave capacity installed. In the non-linked grids case, where the north grid was the only grid affected, the duty cycle of the two largest units only began to decrease when installed wave capacity reached approximately 4 MW. Rather, the duty cycle of the two smaller units decreased initially.

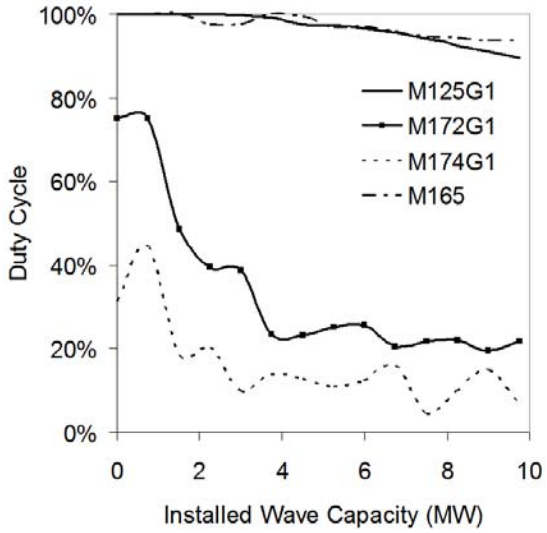

Figure 26: Generator duty cycles vs. installed wave capacity, CD location, non-linked case

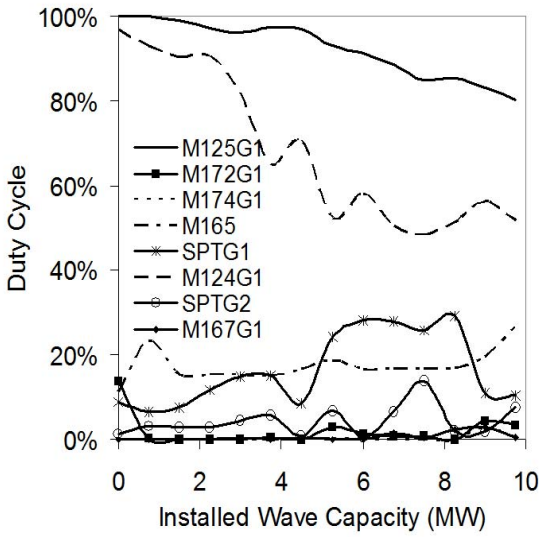

Figure 27: Generator duty cycles vs. installed wave capacity, CD location, linked case

The duty cycle of the diesel generating units behaved similarly in the WM location, however duty cycle decreased more (Figures 28 and 29). The largest change is seen in the linked case where the two largest units decrease 45% and 70% with 9.75 MW of wave capacity installed. The effect on the non-linked grids is much smaller, expressing no clear pattern. In both the linked and non-linked cases, it is evident that the duty cycles of diesel generating units plateau as installed wave capacity increases, indicating that diesel generation cannot be completely replaced with wave energy. This indicates that no further wave energy can be absorbed and, in turn, leads to a steady increase in curtailed wave energy at higher installation levels.

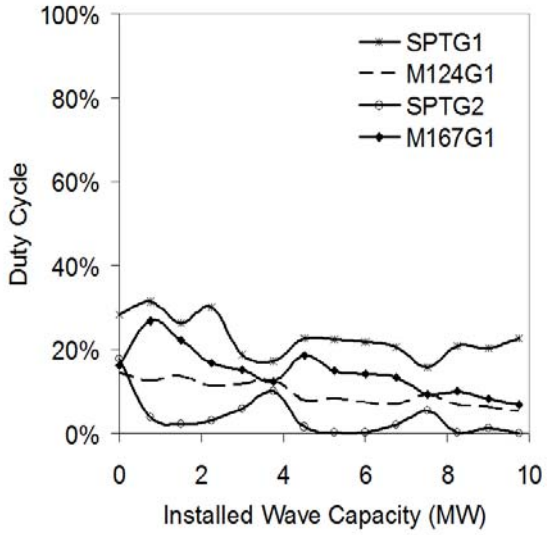

Figure 28: Generator duty cycles vs. installed wave capacity, WM location, non-linked case

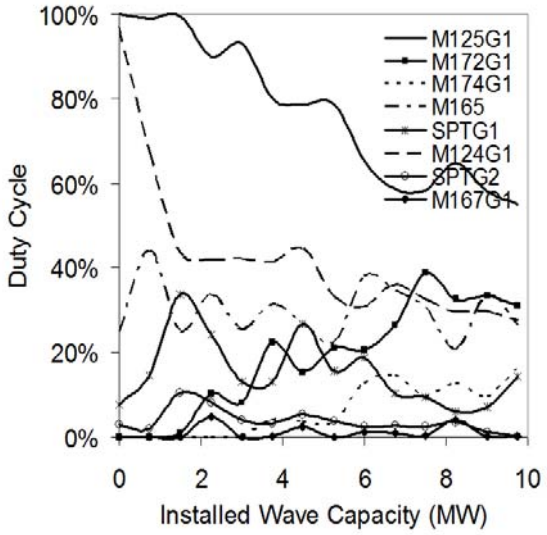

Figure 29: Generator duty cycles vs. installed wave capacity, WM location, linked case

Cycling of the diesel generating units never exceeded the allowable limit of one cycle per day for each unit in either location and either grid configuration. M125G1, the 2.5 MW capacity unit in Masset DGS, cycled most often when the grids were linked for both locations. The maximum number of cycles reached in two weeks for M125G1 was 7 for the CD location and 6 for the WM location when the grids were linked. When the grids were not linked in the CD location, the maximum number of cycles for a generator in the north grid was 5, far below the allowable limit. For the WM location, when the grids were not linked the maximum number of cycles for a generator in the south grid was 3. These results suggest that intermittency of wave energy is not significant enough to drastically increase generator cycling.

The CF of the wave plant was determined in the same manner as that of the tidal plant; the total wave energy used over the two week time period was divided by the theoretical output of the wave plant assuming it had operated at maximum capacity for the entire time. Figure 30 shows the CF for each location and each case. It can be seen that the highest CF is reached for the WM location linked case. Since some wave power is curtailed, the actual CF is slightly lower than the resource CF. Additionally, the resource CF is less than 100% because the device is not always operating at its maximum capacity. It was found that the maximum instantaneous power output that the Pelamis

device reached was 100% of its rated capacity at the WM location and 84% at the CD location. Wave plant CF levels for the WM location non-linked case are far below the resource CF. This is directly a result of the high curtailment of wave energy in that case, which is in turn due to a hydro energy saturated system.

The carbon dioxide emissions of the system with increasing installed wave capacity are shown in Figure 31. Clearly the largest reduction in emissions is seen in the WM location when the grids are linked. Although reductions are seen in the non-linked grids cases, they are always less than if the grids were linked. Nevertheless, emissions for the CD location are not significantly lower for the linked case than the non-linked case, indicating that from an emissions perspective linking the grids will lead to only a slight improvement.

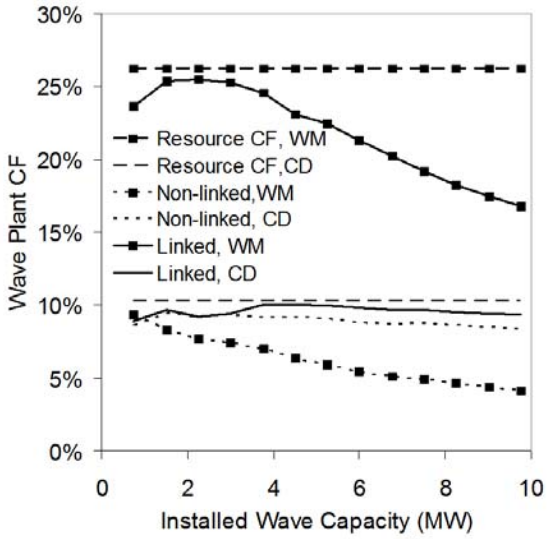

Figure 30: Optimized annual wave plant capacity factor

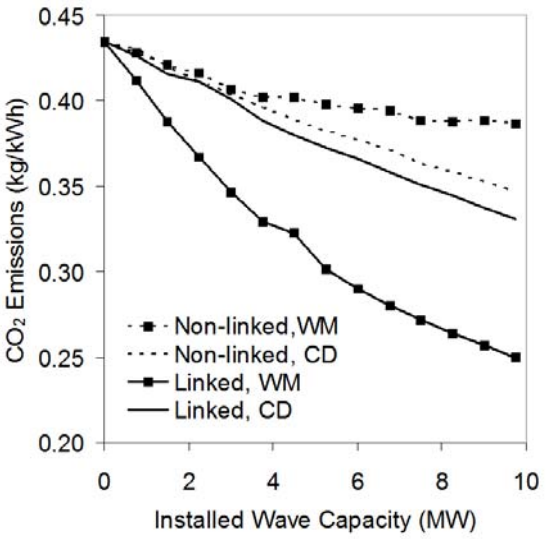

Figure 31: Average CO_2 emissions vs. installed wave capacity

The resulting operational cost of energy for the system with wave power input was determined for each location and each grid configuration (Figure 32). The cost with no installed wave capacity was the same for wave energy input from both locations of course, but as installed wave capacity increased it became clear that the WM location with linked grids has the largest potential to reduce costs. Integrating wave power while not linking the grids had a smaller effect on system cost; however, cost was still reduced for both locations.

The break even project cost was determined from the total annual savings (Figure 33). Once again a project lifetime of 20 years was assumed with a discount rate of 6%. This project cost, although reported in terms of installed wave capacity, encompasses all project costs including capital costs for the wave devices and transmission lines to link the device to the grid, as well as all O&M costs. In the case of wave energy, the capital cost for transmission lines could be quite significant. It is clear that the most economical option is to install WEC devices at the WM location while linking the grids. However, in the event that the grids are not linked, the most economical option would be to install WEC devices at the CD location.

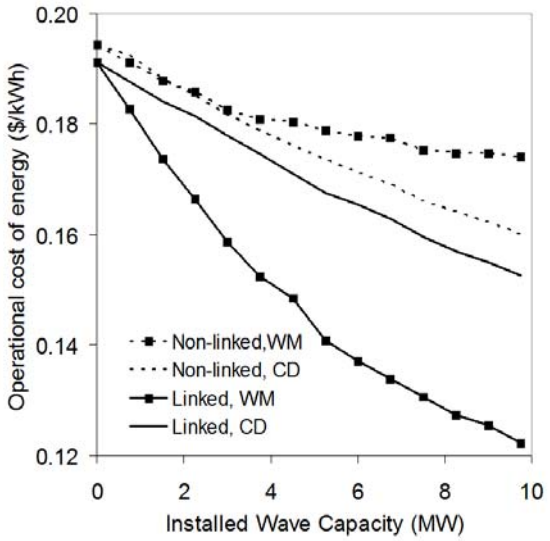

Figure 32: Annual operational cost of energy vs. installed wave capacity

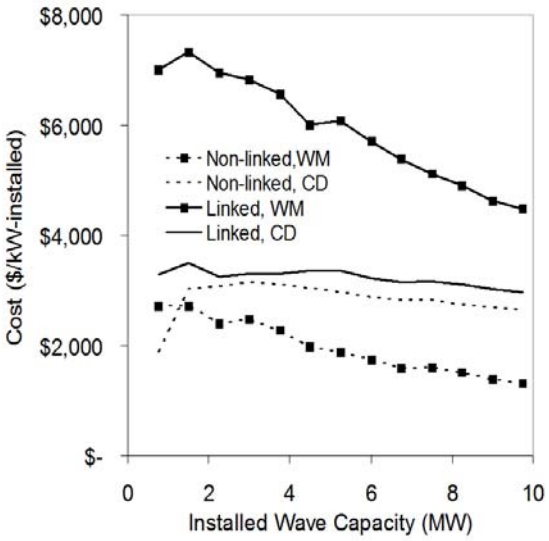

Figure 33: Break even project cost vs. installed wave capacity

Chapter 6

Developing an Operational Strategy

Although optimization results represent the lowest cost solution, they do not necessarily represent the most realistic way of operating the system. It was desired to model a more practical operating scheme based on guidance from optimization results. A major change in the control strategy from the optimization model was making the renewable power must-take by the system. This meant that if renewable power was available, the system must use it before it used diesel generation, a commonly used operational strategy. Curtailment of renewable power was only allowed if it exceeded the remaining load after hydro power had been accounted for or if line constraints were encountered. This chapter outlines the operational strategy developed, as well as system impacts due to the addition of both tidal and wave power.

6.1 A Simulation Model

An operation strategy for energy generation was developed to model operator behaviour realistically. Based on optimization results, strategies were developed for both the linked and non-linked cases. Hydro and renewable power were assumed must-take, with diesel generators meeting the remaining load. Generators were constrained to operate at a minimum of 50% of their rated capacity with no dumping of power allowed. To meet the load at times when the remaining load was less than the minimum operational level of the smallest generator, the smallest generator was allowed to operate below this threshold. Transmission line carrying capacity was included for line d only, as it was found from optimization results to be the only line that constrained the operation of the system. All costs remained the same as those used in the optimization model, and the exact same scenarios were analyzed.

Duty cycle results from optimization determined the order in which generation units would be used. Those with high duty cycles were selected first and those with low duty cycles were selected last. The dispatch order of generators varied for each season analyzed and for the linked versus non-linked cases. Since the largest units were the most often used in all optimization cases, the large units were the first to be selected. The first two generators were base loaded at their minimum operational levels and

subsequently ramped up and down to meet fluctuations in the load. This technique helped limit cycling of generators and most accurately matched the average generation levels from optimization. Following the base loading of the first two units, the rest of the generators were operated at their rated capacity when needed, with the third generator selected before the fourth and so on. A flow chart of the operational policy used is shown in Figure 34 where *G1*, *G2*, and *G3* represent the first, second, and third generators selected respectively. Table 9 shows the generator dispatch order for each case.

The simulation makes a distinction between all units of the same size. However, in practice these units can be used interchangeably. Therefore, rather than limiting the number of cycles of each individual generator, the total number of cycles for all units of one size were considered. For example, in the case of the linked grid the total number of cycles for SPTG1 and SPTG2 should be restricted to be 2 or below for every day, which is equal to cycling once a day each. Including this constraint in the model led to problems with meeting the load with increasing installed renewable capacity. In order to avoid this problem, and gather results for all levels of installed renewable capacity considered, this constraint was not applied to the model. Rather, results were analyzed to see at what level of installed renewable capacity the cycling limit of each generator size group was exceeded.

Table 9: Generator dispatch order

	Linked Case		Non-linked case			
Dispatch order	Generator (all seasons)	Size (MW)	North Grid (Jan & Oct)	North Grid (Apr & Aug)	South Grid (Jan, Apr, Oct)	South Grid (Aug)
1	M125G1	2.5	M125G1	M125G1	SPTG1	M124G1
2	M124G1	2.5	M165	M172G1	SPTG2	SPTG1
3	SPTG1	1.6	M172G1	M174G1	M124G1	SPTG2
4	SPTG2	1.6	M174G1	M165	M167G1	M167G1
5	M165	1				
6	M172G1	0.85				
7	M174G1	0.85				
8	M167G1	0.85				

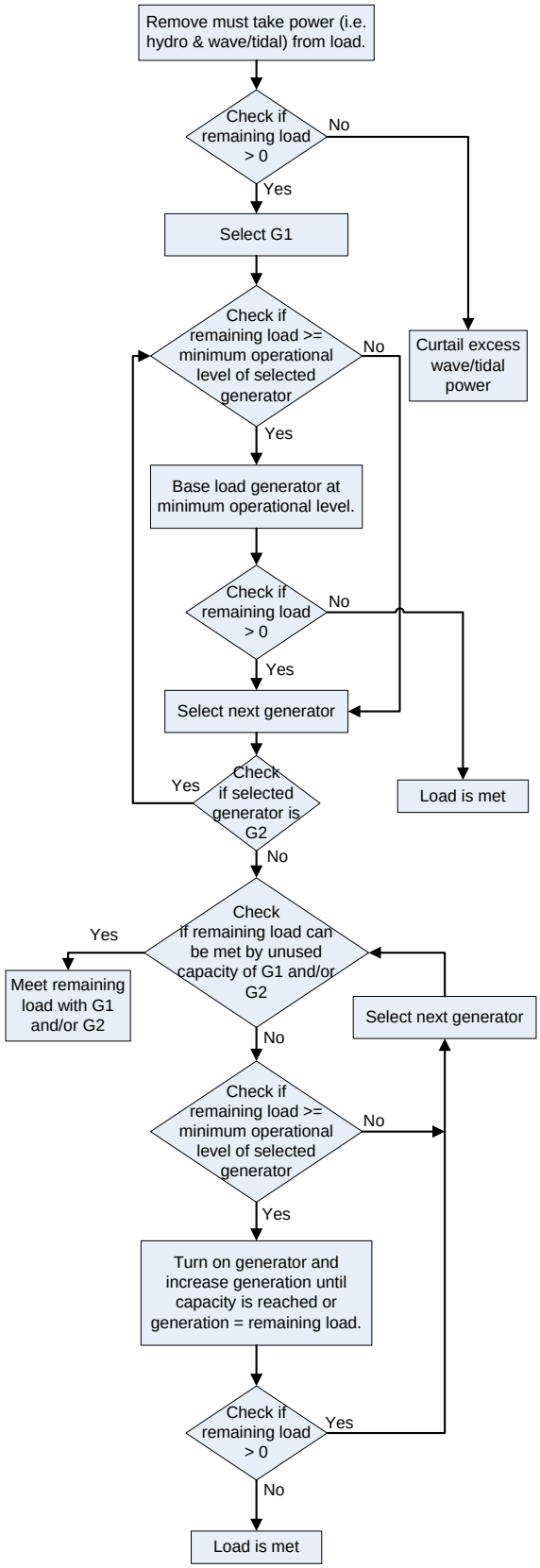

Figure 34: Operational strategy

6.2 The Effects of Tidal Power Addition

Operational strategy simulations were done for both the linked and non-linked cases with zero to 5 MW of installed tidal capacity. Installed tidal capacity was limited to 5 MW as it was felt that this range captured the realistic installation range. In fact, tidal power began to exceed load with 2.2 and 2.8 MW of installed tidal capacity for the non-linked and linked cases respectively. In the absence of storage or curtailment of tidal power, installations above these levels are unlikely.

Duty cycles of the generators show the effects of linking the grid and increasing tidal capacity installed on the operation of each generator (Figure 35 and Figure 36). Linking the grids eliminates the need for the last two generators listed in the linked case dispatch order, M174G1 and M167G1. SPTG2 and M172G1, although not completely out of use, could also likely be removed from operation as they have duty cycles of 1 and 2% respectively. Other generators with higher duty cycles could likely run instead of these units, thereby eliminating the need for four diesel generators if the grids were to be linked. Similar to the optimization results, as installed tidal capacity increased the duty cycle of the larger units decreased. The duty cycle of M125G1 decreased from 100% with no installed tidal capacity to 62% and 47% for the linked and non-linked cases respectively with 5 MW of installed tidal capacity. For the linked case, duty cycles of smaller units held fairly steady with increasing tidal capacity at low values (<10%). In the non-linked case, the duty cycle of M174G1 similarly remained low and the southern grid generators were not affected by increasing installed tidal capacity.

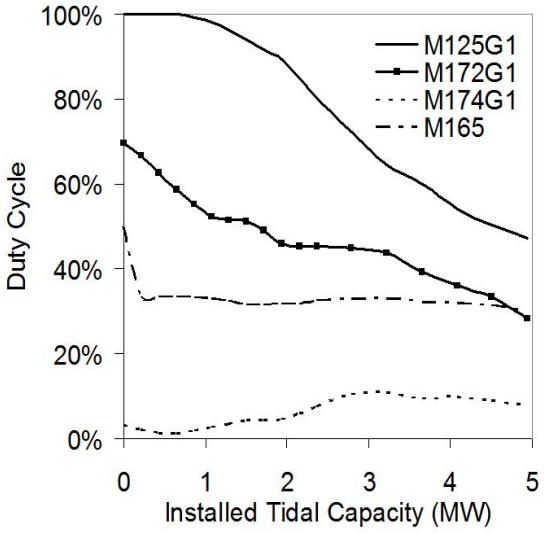

Figure 35: Simulation diesel generator duty cycle vs. installed tidal capacity, non-linked case

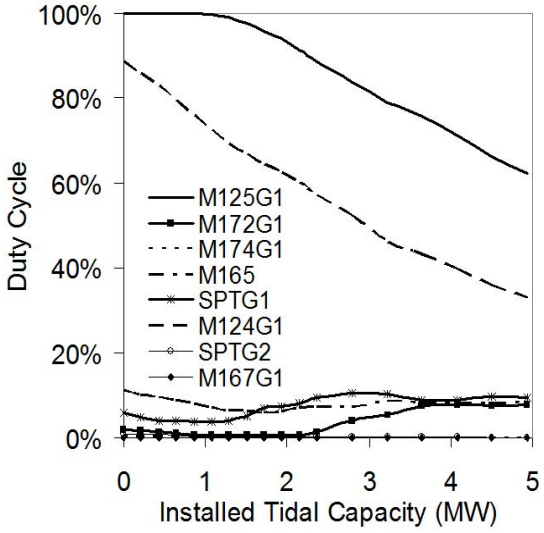

Figure 36: Simulation diesel generator duty cycle vs. installed tidal capacity, linked case

The main difference in results between the linked and non-linked cases was the number of cycles for the diesel generating units. It was found that the non-linked system cycled far more, with the two 850 kW units located at Masset DGS exceeding the maximum number of allowable cycles when installed tidal capacity equalled 1 MW. On the other hand, the generating units in the linked case did not exceed the allowable number of cycles until installed tidal capacity reached 1.7 MW, at which point the two 2.5 MW units cycled more than allowed. This situation could likely be avoided through a change of dispatch order, extending the allowable installed tidal capacity. In the non-linked case, the north grid has fewer generators to choose from and as a result exceeded allowable cycling for all generators when installed tidal capacity equalled 2 MW. The same point is never reached for the linked case. This suggests that from an operational perspective no more than 2 MW can be installed in the non-linked system with such an operating strategy. On the other hand, if the grids were linked this feasible level of installed tidal capacity could rise to 5 MW.

Since no dumped power is allowed, and tidal power is considered must-take, diesel generation is equal for the linked and non-linked cases until tidal power begins to exceed the north grid load. Similarly, tidal energy used is equal for both cases until it exceeds the load. At that point, less tidal energy can be absorbed by the separate grid system than

the linked system. Figure 37 shows diesel generation, tidal energy used, and curtailed tidal energy normalized by total diesel generation with no renewable input, as was done previously for the optimization results. Generation for the two cases does not noticeably deviate until installed tidal capacity exceeds 3 MW. Average annual tidal plant CF is, likewise, the same for both cases until tidal power begins to exceed load. As mentioned before, this occurs at 2.2 and 2.8 MW installed capacity for the non-linked and linked cases respectively. Figure 38 illustrates the decrease in CF at these points.

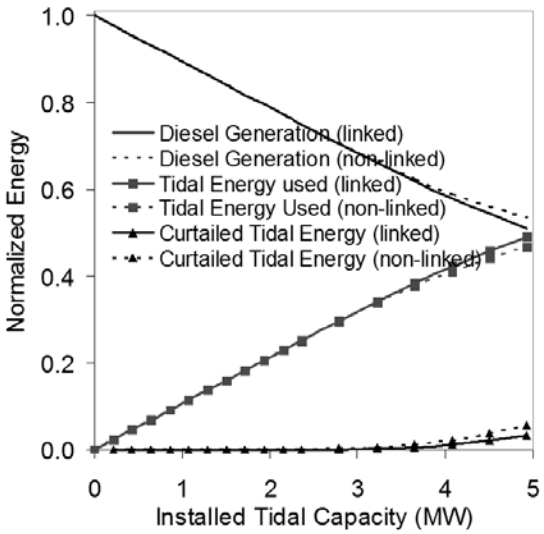

Figure 37: Simulation energy contribution by source vs. installed tidal capacity

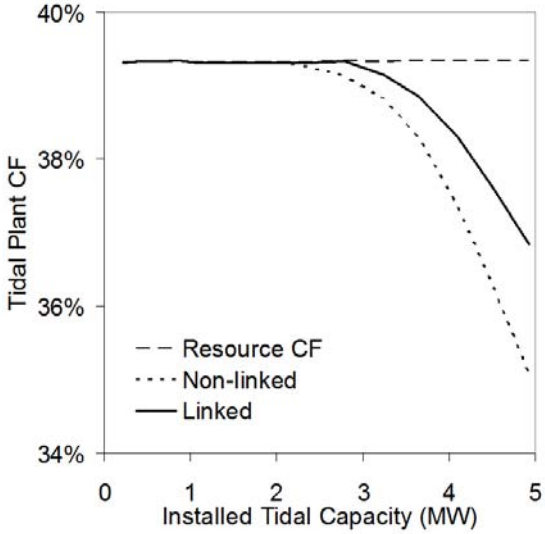

Figure 38: Simulation average tidal plant capacity factor

Comparing simulation to optimization results shows the effects of the operational strategy on tidal energy absorbed and diesel generator cycling. Tidal power was not considered must-take in the optimization, therefore leading to higher curtailed tidal energy values. Figure 39 shows curtailed tidal energy in the linked and non-linked cases for both the optimization and simulation normalized by total diesel generation with no renewable input. Curtailed tidal energy is always higher in the optimization. On the other hand, Figure 40 shows the total number of cycles in both cases for the optimization and simulation, and it can be seen that the number of diesel generating unit cycles is far higher for the simulation. This indicates that curtailing a bit of tidal energy leads to less cycling of diesel generators.

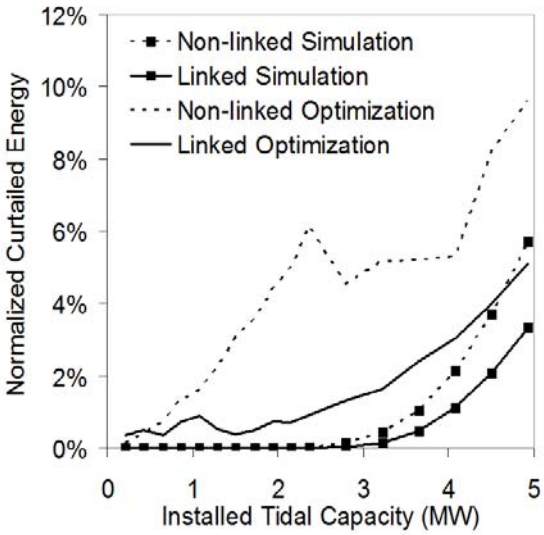

Figure 39: Curtailed tidal energy vs. installed tidal capacity

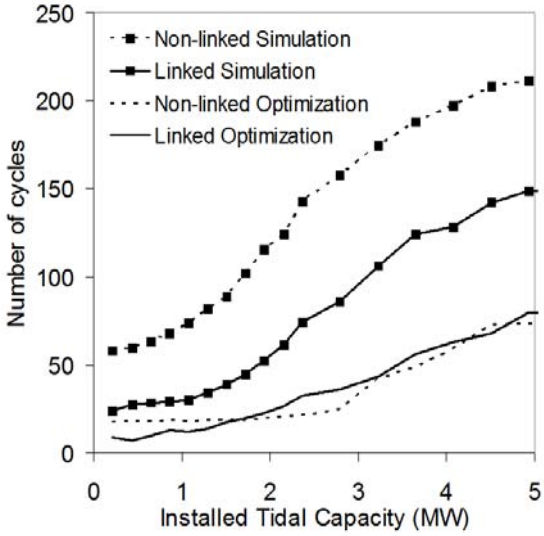

Figure 40: Total number of diesel generator cycles vs. installed tidal capacity

Simulation results were used to determine reductions in emissions and costs, as well as break even project costs, with increasing installed tidal capacity. The decrease in emissions is linear and equal for both the linked and non-linked cases until excess tidal energy is present (Figure 41). Regardless, the level of excess tidal energy is not large enough to significantly alter the trend for the linked case. Figure 37 shows graphically the relatively small amount of curtailed tidal energy to load. The operational cost of energy for the simulation is slightly higher for the non-linked case than the linked case for all levels of installed tidal (Figure 43). This occurs because the generators are operating at lower part loads in the non-linked case, which is more expensive on a per energy unit basis. Also, the diesel generators often cycled at or near their allowable limit in the non-linked case. This is unlikely to be the way the generators are operated, indicating that the cost could be overestimated due to high cycling costs. The annual savings due to linking the grid are estimated at approximately $415,000.

The break even project cost was determined in the same manner for the simulation as was done for the optimization (Figure 42). At all installed tidal capacity levels, it is more economical to integrate tidal power if the grids are linked. The break even cost is initially on the order of 10,000 $/kW-installed for the linked grids case and approximately 500 $/kW-installed less for the non-linked grids. However, as installed

tidal capacity increases the break even cost decreases for both cases, with the most significant decrease seen in the non-linked case.

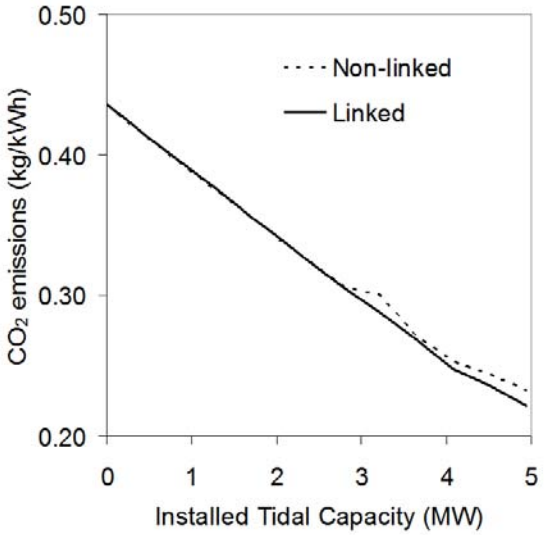

Figure 41: Simulation average CO_2 emissions vs. installed tidal capacity

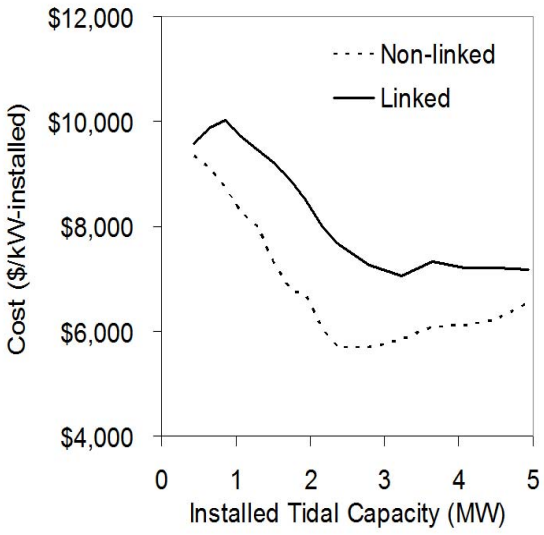

Figure 42: Simulation break even project cost vs. installed tidal capacity

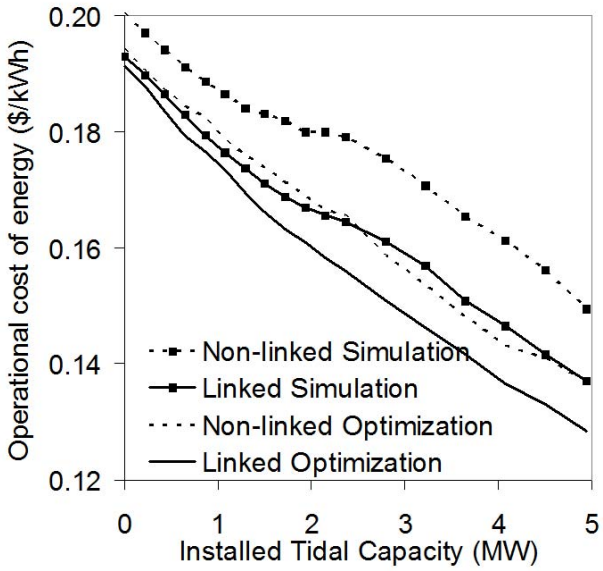

Figure 43: Annual operational cost of energy vs. installed tidal capacity, all cases

6.3 The Effects of Wave Power Addition

The effects of integrating wave power into the Haida Gwaii system under the developed operational strategy were explored for both locations: CD and WM. As stated

before, significantly more wave energy is available in the WM location than the CD location with the same installed capacity due to the differences in resource CF (Table 5). However, integration of wave power from the WM location was shown from optimization results to be limited due to carrying capacity constraints on line d of the grid. As wave power is assumed must-take by the operational strategy, it is only curtailed when it exceeds the load or is limited by line carrying capacity. Figure 44 and Figure 45 show the diesel energy generated, wave energy used, and wave energy curtailed for each location when using the operational strategy. Once again these values have been normalized by total diesel generation with no renewable input, representing the remaining load after hydro energy has been absorbed, which is also the load that must be currently met by diesel generating units. It can be seen that results are very similar to optimization results.

Very little wave energy is curtailed using the control strategy at the CD location, while at the WM location significant wave energy is curtailed for both the linked and non-linked grids case. Wave energy from the CD location begins to exceed load with 6 MW of capacity installed for both grid configurations. However, curtailed values are almost negligible. With wave energy input from the WM location, if the grids are not linked wave power is immediately curtailed, and if the grids are linked wave power is curtailed when installed wave capacity exceeds 2.25 MW. In almost all cases the curtailed wave energy is higher for the optimization results than the simulation. The only exception is the non-linked case with wave energy input from the WM location, where curtailed power is equal above 6MW of installed wave capacity. The curtailed energy from the optimization results is within 5% of the simulation levels, showing that curtailment of wave energy is rarely chosen by the optimization model unless load is exceeded or a line constraint is met.

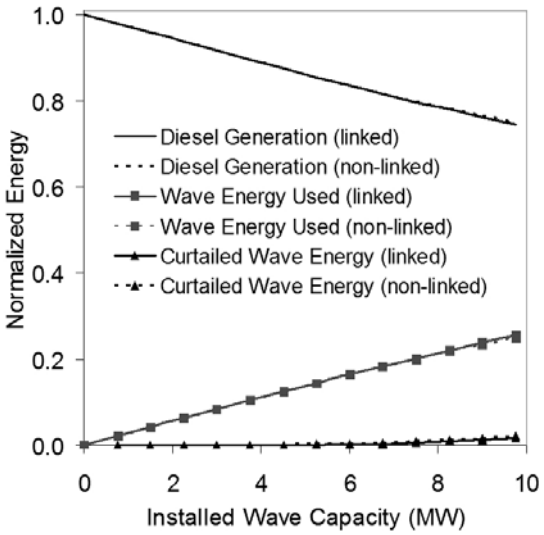

Figure 44: Simulation energy contribution by source vs. installed wave capacity, CD location

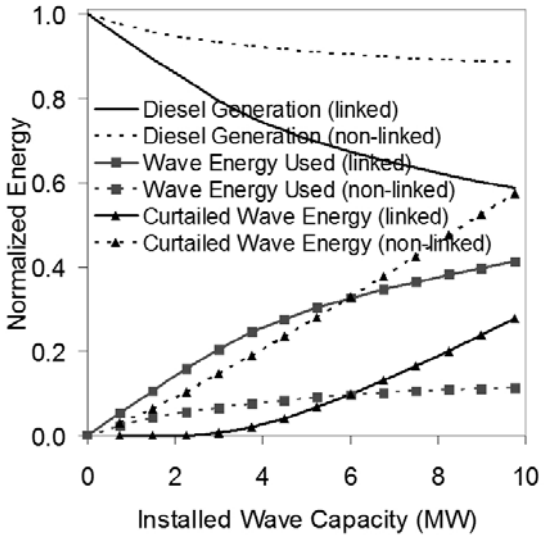

Figure 45: Simulation energy contribution by source vs. installed wave capacity, WM location

Figure 46 shows the CF of the wave plant for all situations, and it can be seen that results are slightly higher than those from the optimization (shown in Figure 30). This, of course, occurs due to the must-take strategy imposed on wave power, leading to higher plant CF values at equal levels of installed wave capacity. Reductions in CF are seen with increasing installed capacity due to the increased curtailment of wave power. The point where wave energy exceeds load can be seen in Figure 46 as well, as the plant CF deviates from the resource CF. As mentioned previously, this occurs with 6 MW of wave capacity installed for input from the CD location for both grid configurations. Wave input from the WM location immediately exceeds the load when the grids are not linked and does so with 2.25 MW installed for the linked grid configuration.

Cycling of the diesel generators, although not an issue for the optimized results, became a problem when utilizing the control strategy. Figure 47 shows the total number of cycles for all diesel generating units when wave energy was input from both the CD and WM location. When wave power was input from the CD location, no cycling limits were exceeded for the linked case, but were exceeded when installed wave capacity reached 8.25 MW for the non-linked case. Wave power input from the WM location never led to over cycling of the diesel generating units for either the linked or non-linked case. In fact, cycling was actually reduced for the non-linked case as duty cycles of

generating units tended towards zero with increasing installed wave capacity. It is clear that increasing installed wave capacity tends to increase the number of cycles. Furthermore, the non-linked case usually has a higher number of cycles than the linked case.

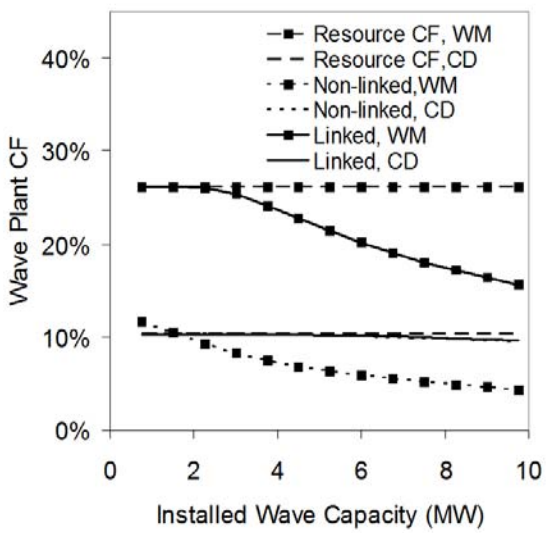

Figure 46: Simulation wave plant annual CF

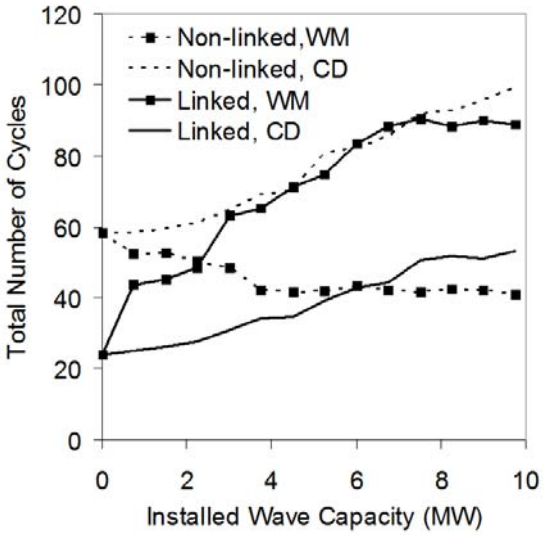

Figure 47: Simulation total number of cycles vs. installed wave capacity

The operational cost of energy with increasing wave capacity while using the operational strategy is shown in Figure 48. The largest savings can clearly be achieved for the linked grid case with wave energy input from the WM location. Cost for the non-linked case with input from the WM location shows that cost plateaus and only slight savings can be achieved above 3.75 MW of wave capacity installed. Steady cost decreases are seen for both linked and non-linked grids with input from the CD location due to the low curtailment of wave energy. Carbon dioxide emissions follow the same pattern since fuel consumption, cost and emissions are all directly related. Costs for the simulation are all higher than energy costs from the optimization.

The project break even cost in terms of kW of wave power installed is shown in Figure 49. It indicates that the most economical option would be installation of wave power in the WM location to a linked grid system. The maximum break even cost occurs with 2.25 MW of wave capacity installed from the WM location at a level of 5,900 $/kW-installed. In the situation where the grids are not linked, it appears that installation of

wave power at the WM location would be most economical below 3.75 MW installed, switching to the CD location above this level. Furthermore, installing wave power into the non-linked system would be most economical at low levels of installed capacity. As mentioned previously, the break even cost includes all O&M and capital costs associated with offshore transmission lines linking the device to the grid, costs which could be quite significant.

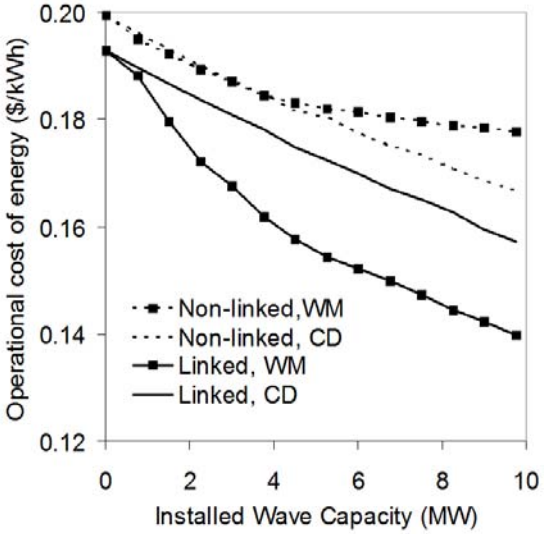

Figure 48: Simulation annual operational cost of energy vs. installed wave capacity

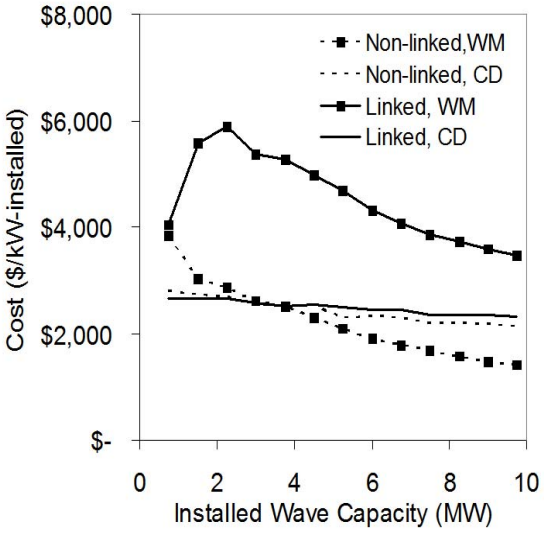

Figure 49: Simulation break even project cost vs. installed wave capacity

6.4 Comparison of Wave and Tidal Power

Comparisons of wave and tidal power were done individually for operational strategy simulations results of the linked and non-linked cases. Overall, the linked case appeared more viable as the break even project costs were higher and the diesel generator cycling was less frequent. Figure 50 shows the diesel generation contribution to the load normalized by the contribution with no renewable capacity installed for the linked case. It is apparent that the tidal energy option will replace more diesel generation than wave energy. However, the total numbers of diesel generator cycles are seen, for the linked case, in Figure 51 and it is clear that tidal energy input would lead to a significant increase in the number of cycles. In fact, the allowable number of cycles for the linked

case with tidal input is exceeded with 1.7 MW installed. The maximum number of allowable cycles is never exceeded when wave energy is input from the WM location. On the other hand, curtailed energy is always higher for the case of wave energy input from the WM location than tidal energy input, a finding which is directly due to the limited carrying capacity of line d.

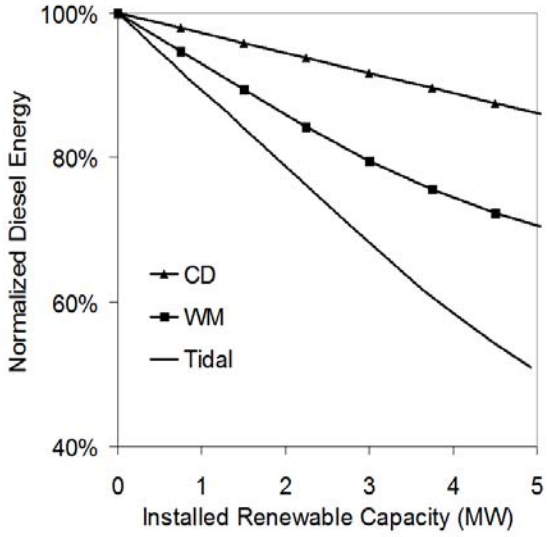

Figure 50: Diesel energy generated with all renewable options, linked grid with operational strategy

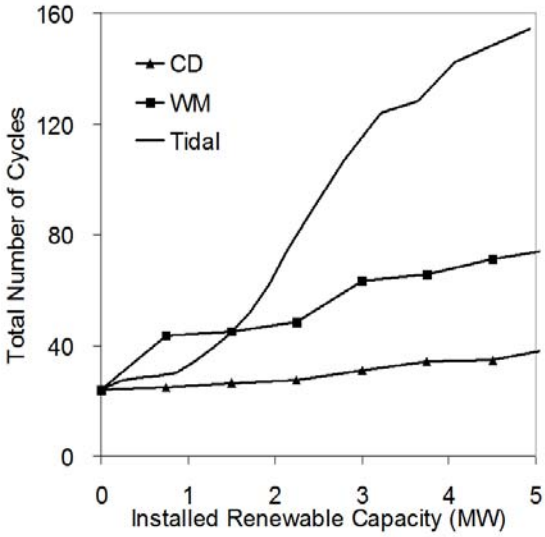

Figure 51: Total number of diesel generator cycles with all renewable options, linked grid with operational strategy

Operational cost of energy and break even project cost for all renewable energy options with a linked grid are shown in Figure 52 and Figure 53. Tidal energy appears to be the lowest cost option and Figure 53 follows this by showing tidal to have the highest project break even cost at approximately 10,000 $/kW-installed. The maximum break even project cost for wave energy input from the WM location is 5,900 $/kW-installed, considerably lower than tidal energy. In the event that the carrying capacity on line d was increased to the point where it no longer affected system operation, meaning no wave energy was curtailed unless it exceeded the load, the maximum break even cost of wave energy from the WM location increased to 6,800 $/kW-installed. This value is still lower than that of tidal energy due to the lower resource CF available. Furthermore, the additional capital cost required for transmission for the offshore wave plant will likely be higher than transmission costs for the tidal plant as it will be farther offshore. This

results in an even larger gap between maximum allowable capital costs of the devices alone.

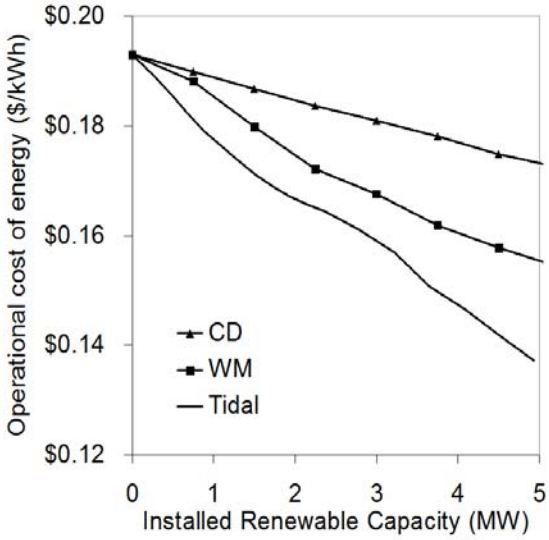

Figure 52: Annual operational cost of energy with all renewable options, linked grid with operational strategy

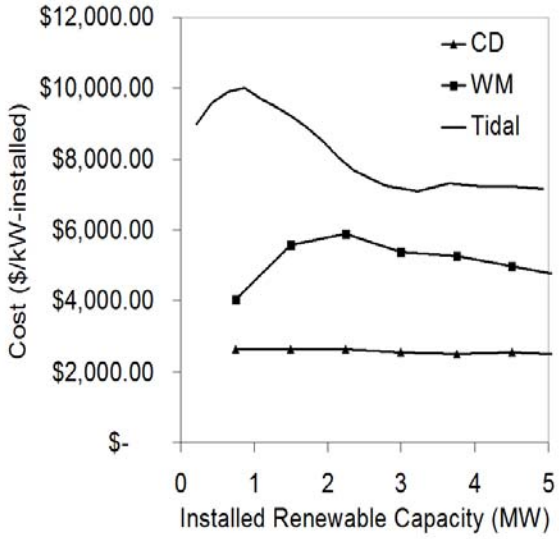

Figure 53: Break even project cost with all renewable options, linked grid with operational strategy

Results from the non-linked cases clearly show that tidal power would be the lowest cost option and wave power would likely not be suitable if the grids were not linked (Figure 54 and Figure 55). A low CF for the CD location and a south grid already saturated with cheap hydro power contribute to this result. Levels of diesel generation are 11% lower when tidal power is input rather than wave power at a level of 1.5 MW of renewable capacity installed, and 33% lower with 5 MW installed. However, tidal power proves to be more problematic for generator cycling when the grids are not linked, causing them to cycle more than their limit with only 1 MW installed. Wave energy, on the other hand, does not cause generating units to exceed their allowable number of cycles until 8.25 MW is installed in the CD location, and never does so for the WM location.

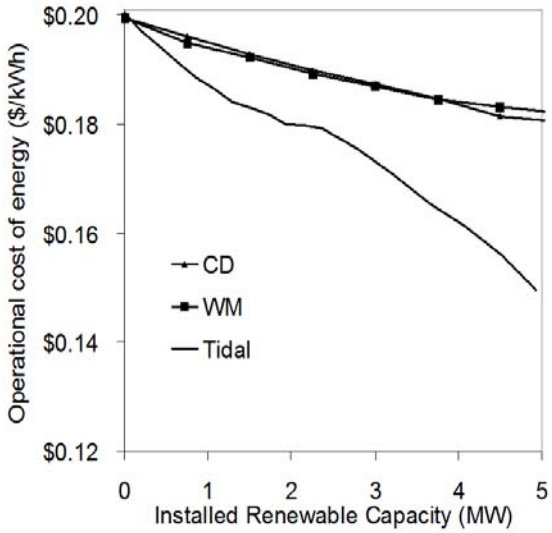

Figure 54: Annual operational cost of energy with all renewable options, non-linked grid with operational strategy

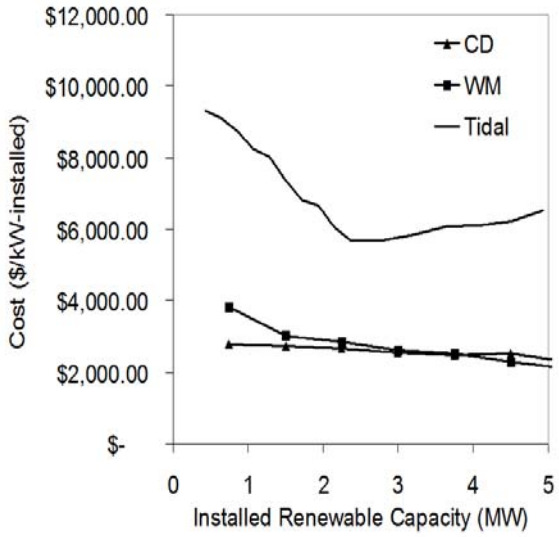

Figure 55: Break even project cost with all renewable options, non-linked grid with operational strategy

Chapter 7

Conclusions

The issue of integration of renewable power is of significant interest for remote communities with high costs of electricity. Haida Gwaii, a remote archipelago off the northwest coast of British Columbia, Canada, faces a rising cost of electricity due to its dependence on fossil fuels for energy generation. To understand the impact of renewable energy integration, with regards to cost, emissions, and system operation, an optimization network model was built. GAMS was used to develop a linear mixed integer model which was accompanied by a Matlab interface. The current generation system on Haida Gwaii consists of two separate grids, north and south, each supplying a peak load on the order of 5 MW. The option of linking the grids was analyzed along with the impact of integrating both tidal and wave energy. An operational strategy simulation model for the generation system was developed based on the optimization results in order to model more realistic practices, in which renewable power was considered must-take.

7.1 Key Findings

Linking the grids was found to reduce the number of diesel generators in operation, frequency of cycling the diesel generators in operation, system emissions, and cost of electricity. The optimal average annual cost of electricity dropped from 0.194 $/kWh to 0.191 $/kWh by linking the grids. From this, annual savings from the optimization model were found to be on the order of $175,000 CAN. Operational strategy model results found the average annual cost of electricity to be slightly higher than that from the optimization model at 0.200 $/kWh for the non-linked case and 0.193 $/kWh for the linked case, resulting in annual savings of $415,000 CAN.

Tidal energy integration from Masset Sound was analyzed for installed capacities of 0.22 MW to 9.85 MW, or power penetration levels of 2.2% to 100% for the linked grids case and 4.6% to 206% for the non-linked grids case. These levels corresponded to maximum energy penetration values of 55% and 130%, respectively. Tidal power input was found to increase the number of diesel generating units in operation as well as the frequency of cycling of the units. Due to an operational policy of not cycling each diesel generating unit more than once a day, it was found that the minimum cost solution from

the optimization model results could not be followed above 2.5 MW of tidal capacity installed for the non-linked case and 3.2 MW for the linked case. Following an operational policy further reduced this feasible operating limit to be 1 MW and 1.7 MW of tidal capacity installed for the non-linked and linked cases, respectively.

Carbon dioxide emissions and cost of electricity decreased almost linearly as installed tidal capacity increased from 0 to 4 MW for the optimization model, resulting in savings of 0.054 and 0.051 $/kWh for the linked and non-linked cases respectively. Above this level of tidal capacity installed, diminishing returns were seen. Slightly lower savings of 0.046 and 0.039 $/kWh were determined from the simulation model for the linked and non-linked cases respectively with 4 MW of tidal capacity installed.

Project break even costs for a tidal plant, calculated based on a 20 year project life, 6% discount rate, and including all operational and maintenance and transmission costs, were constantly higher for the linked case than the non-linked case. The maximum break-even cost for the linked case from the optimization model was found with 0.65MW of tidal capacity installed at 11,500 $/kW-installed, and at 0.86 MW installed and 10,000 $/kW-installed from the simulation model. Such findings suggest that it is both economically and technically beneficial to link the grids before integrating tidal power while maintaining low levels of installed tidal capacity.

The impacts of wave energy integration were explored for two different locations, Central Dixon Entrance and West Moresby. Central Dixon Entrance, located 40 km offshore from the town of Masset, had an average annual resource capacity factor of 10% when using the Pelamis device selected. West Moresby was located more remotely, 45 km off the western shore of Moresby Island, but benefitted from an average annual resource capacity factor of 26% with the Pelamis device. Installation levels investigated included 1 – 13 Pelamis devices sized at 750 kW each, resulting in maximum power penetrations of 99 and 204% for the linked and non-linked grids respectively. Integration of wave energy was found to increase the number of diesel generating unit cycles, however never caused a single unit to cycle more than its allowable daily limit, a positive result from the system operation point of view. Optimization and simulation results found that integration of wave energy from the West Moresby location to a linked grid would be the most economical option. Maximum project break even costs for such a

scenario were found to be 7,300 and 5,900 $/kW-installed for the optimization and simulation models respectively. However, it was clear that above 2.25 MW of wave capacity installed, or 3 Pelamis devices, the carrying capacity of the submarine cable linking Moresby Island to Graham Island would limit the wave energy penetration level. Above this level of installed wave capacity wave energy would need to be curtailed, indicating that upgrading the submarine cable or some form of storage would be beneficial.

7.2 Recommendations

Linking the grids was shown to reduce system operating costs and improve system operation. Simulation results looking at a linked versus non-linked grid indicated that at least two diesel generating units would not be required, and two others were used less that 2% of the year each when the grids were linked. Furthermore, cycling of diesel generating units would decrease by 59%. Annual savings estimated from the simulation model as a result of linking the grids were approximately $415,000 CAN. However, it was clear that the submarine cable linking Moresby Island to Graham Island would be a bottleneck in the system should the grids be linked, limiting the amount of energy Sandspit DGS would be able to send to Graham Island. This indicates that linking the grid should consider not only the cost of the new line but also of upgrading the submarine cable.

The question of whether wave or tidal energy is a better option to integrate into the Haida Gwaii system is dominated by two issues: system operation and cost. Both optimization and simulation results indicate that from a system operational perspective wave energy is a more favourable choice to integrate than tidal energy. This is chiefly due to the fact that less cycling of diesel generating units is needed thanks to a more consistent resource. In fact, current system operational constraints limit the feasible installation range of a tidal plant in Masset Sound to be at maximum 1 MW, increasing to 1.7 MW if the grids were to be linked. On the other hand, a wave plant in the Central Dixon Entrance location is limited to 8.25 MW installed when input into the north grid, while all other wave energy scenarios investigated were not found to be limited by diesel generating unit cycling constraints.

From a cost perspective it is clear that integrating tidal energy is a better option. Additionally, it is clear that it is more economical to integrate renewable power if the grids are linked and installed levels remain low. Break even project cost estimates from the simulation model for the tidal plant with a linked grid were on the order of 10,000 $/kW-installed for 1 MW installed. The highest break even project costs for a wave plant were for the West Moresby location with a linked grid and were on the order of 6,000$/kW-installed for 2.25 MW installed. The discrepancy between the two values is largely due to the lower annual capacity factor of the wave power resource as compared to the tidal power resource, namely 26% as opposed to 39%. Furthermore, the break even project cost includes the cost associated with transmission of the power to shore, and since the wave plant is likely to the farther offshore that capital cost will be higher. This, in turn, increases the gap between maximum allowable capital cost for the tidal and wave energy devices alone.

Further development of the network model should be done to fully understand the possible impact of renewable power integration. Up to this point, hydro power from Moresby Lake Hydro Facility has been assumed must-take with no storage capabilities. A dynamic reservoir model should be developed for the facility, from which the option of including storage could be explored. Other storage options could also be considered, such as pumped hydro or battery storage. The information provided with regards to transmission lines was limited, therefore resulting in a simplified grid. More detailed information on the transmission lines would allow for a more complete representation of the network. Furthermore, a full AC power analysis of the grid would provide a more realistic solution as reactive power, voltage fluctuations, and phase angles would be accounted for. Although it is unlikely that an optimization model will be able to solve for a period of one year, the simulation model could be run for an entire year rather than four separate two week periods. Possible future costs relating to the production of carbon dioxide emissions could also be included in the model, an interesting consideration for future policy makers. Finally, other renewable energy options, such as wind or biomass, could be similarly analyzed with the model and compared.

Bibliography

1. Weisser, Daniel, and Raquel S. Garcia. "Instantaneous Wind Energy Penetration in Isolated Electricity Grids: Concepts and Review." Renewable Energy 30.8 (2005): 1299-308.

2. Sheltair Group. Haida Gwaii Community Electricity Plan. April 2008.

3. BC Hydro. Personal Communication. June 2008.

4. Cornett, A. Inventory of Canada's Marine Renewable Energy Resources. Canadian Hydraulics Centre, National Research Council of Canada; April 2006. CHC-TR-041.

5. Triton Consultants Ltd. Canada Ocean Energy Atlas (Phase 1) Potential Tidal Current Energy Resources Analysis Background. Prepared for the Canadian Hyrdaulics Centre, May 2006.

6. Government of Germany. "Amendment of the Act on Granting Priority to Renewable Energy Sources: English Edition." April 2, 2004.

7. Gross, R., et al. "Renewables and the Grid: Understanding Intermittency." Proceedings of the Institution of Civil Engineers. Engineering sustainability 33 (2007): 31-41.

8. Jebaraj, S., and S. Iniyan. "A Review of Energy Models." Renewable and Sustainable Energy Reviews 10.4 (2006): 281-311.

9. Joshi, Bharati, T. S. Bhatti, and N. K. Bansal. "Decentralized Energy Planning Model for a Typical Village in India." Energy 17.9 (1992): 869-76.

10. Malik, B., et al. "Mathematical Model for Energy Planning of Rural India." International journal of energy research 18.4 (1994): 469-82.

11. Iniyan, S., and K. Sumathy. "An Optimal Renewable Energy Model for various End-Uses." Energy 25.6 (2000): 563-75.

12. Kaldellis, J. K., and K. A. Kavadias. "Optimal Wind-Hydro Solution for Aegean Sea Islands' Electricity-Demand Fulfilment." Applied Energy 70.4 (2001): 333-54.

13. Muckstadt, John A., and Sherri A. Koenig. "An Application of Lagrangian Relaxation to Scheduling in Power-Generation Systems." Operations research 25.3 (1977): 387.

14. Uri, N. D., and S. Hassanein. "Modeling the High Frequency Demand for Energy." Applied Energy 19.1 (1985): 49-59.

15. Uri, N. D. "Forecasting Peak System Load using a Combined Time Series and Econometric Model." Applied Energy 4 (1978): 219-27.

16. Weisser, D. "A Wind Energy Analysis of Grenada: An Estimation using the 'Weibull' Density Function." Renewable Energy 28.11 (2003): 1803-12.

17. Hsu, George J. Y., and Feng-Ying Chou. "Integrated Planning for Mitigating CO2 Emissions in Taiwan: A Multi-Objective Programming Approach." Energy Policy 28.8 (2000): 519-23.

18. Weis, Timothy M., and Adrian Ilinca. "The Utility of Energy Storage to Improve the Economics of wind–diesel Power Plants in Canada." Renewable Energy 33.7 (2008): 1544-57.

19. Kaldellis, J. K. "The Wind Potential Impact on the Maximum Wind Energy Penetration in Autonomous Electrical Grids." Renewable Energy 33.7 (2008): 1665-77.

20. Maddaloni, Jesse D., Andrew M. Rowe, and G. Cornelis van Kooten. "Wind Integration into various Generation Mixtures." Renewable Energy 34.3 (2009): 807-14.

21. Bakos, George C. "Feasibility Study of a Hybrid wind/hydro Power-System for Low-Cost Electricity Production." Applied Energy 72.3-4 (2002): 599-608.

22. Hatch Energy. Haida Gwaii/Queen Charlotte Islands Demonstration Tidal Power Plant Feasibility Study. March 2008.

23. Thurman, Harold V. Introductory Oceanography. 8th ed. Upper Saddle River, NJ: Prentice Hall, 1997.

24. Thomson, Richard E. Oceanography of the British Columbia Coast. Ottawa, Ont: Canada Dept. of Fisheries and Oceans, 1981.

25. Garrett, Chris, and Patrick Cummins. "Generating Power from Tidal Currents." Journal of Waterway, Port, Coastal & Ocean Engineering 130.3 (2004): 114-8.

26. Garrett, Chris, and Patrick Cummins. "The Power Potential of Tidal Currents in Channels." Proceedings of the Royal Society 461 (2005): 2563-72.

27. Blanchfield, J., C. Garrett, and A. Rowe. "Tidal Stream Power Resource Assessment for Masset Sound, Haida Gwaii." Proceedings of the Institution of Mechanical Engineers Part A Journal of Power and Energy 222.A5 (2008): 485.

28. Twidell, John, and Anthony D. Weir. Renewable Energy Resources. 2nd ed. London; New York: Taylor & Francis, 2006.

29. Cruz, João. Ocean Wave Energy: Current Status and Future Perspectives. Illustrated ed. Springer, 2008.

30. EPRI. E2I EPRI Assessment. Offshore Wave Energy Conversion Devices. 2004.

31. Finavera Renewables. "Wave Tech: System Configuration." 2007. <http://www.finavera.com/en/wavetech/configuration>.

32. Weinstein, Alla. AquaEnergy Group Ltd. "AquaBuOY in Portugal." <http://ec.europa.eu/research/energy/pdf/gp/gp_events/ocean_energy/1145_aquabuoy_demo_plant_en.pdf>.

33. Finavera Renewables. "Press Room." 2009. < http://www.finavera.com/en/press>.

34. Renewable Energy World. "While Finavera's Buoy Sinks, Hopes of Harnessing Ocean Energy Survive" November 8, 2007. <http://www.renewableenergyworld.com/rea/news/article/2007/11/while-finaveras-buoy-sinks-hopes-of-harnessing-ocean-energy-survive-50510>

35. Pelamis Wave Power. "Pelamis P-750 Wave Energy Converter Brochure." <http://www.pelamiswave.com/content.php?id=161>.

36. Pelamis Wave Power. 2009 < http://www.pelamiswave.com/index.php>

37. Wave Dragon. 2009 <http://www.wavedragon.net/>

38. Marine Environmental Data Services, Department of Fisheries and Oceans Canada. "IdxMap - SVG Data Search." 2008-06-12 2008. <http://www.meds-sdmm.dfo-mpo.gc.ca/meds/Databases/WAVE/idxMAP/idxMapQbasic_e.asp>.

39. Dunnett, David, and James S. Wallace. "Electricity Generation from Wave Power in Canada." Renewable Energy 34.1 (2009): 179-95.

40. Weinstein, A., et al. "AquaBuOY - the Offshore Wave Energy Converter Numerical Modeling and Optimization." Oceans '04. MTTS/IEEE Techno-ocean '04, 4 (2004): 1854-1859.

41. Google. "Google Maps Canada." 2009. <http://maps.google.ca/maps?tab=ml>.

42. Maddaloni, Jesse D. Techno-Economic Optimization of Integrating Wind Power into Constrained Electric Networks. Master of Applied Science University of Victoria, 2007.

43. Alcan Cable. “Bare Overhead Cable. Canadian Product Catalogue.” <http://www.cable.alcan.com/alcancable/en-US/Products/Canada/Bare+Overhead+Conductors/Bare+Overhead+Conductor.htm>

44. Aluminum Association. “Aluminum Electrical Conductor Handbook.” New York (1971).

45. Matt Clare. Finning (Canada) Inc. Personal Communication. December 2008.

46. Diesel Service and Supply Inc. Approximate Fuel Consumption Chart. 2008 <www.diselserviceandsupply.com>.

47. Lefton S.A., Besuner P.M., Grimsrud G.P., “Managing utility power plant assets to economically optimize power plant cycling, costs, life, and reliability,” Proceedings of the 4th IEEE Conference on Control Applications (Cat. No.95CH35764) (1995): 195-208.

48. US Environmental Protection Agency. “Emission Facts: Average Carbon Dioxide Emissions Resulting from Gasoline and Diesel Fuel.” 2008 <http://www.epa.gov/OTAQ/climate/420f05001.htm>.

49. Brooke, A., et al. "GAMS: The Solver Manuals." Washington, DC: GAMS Development Corporation (2005).

50. BC Hydro and Power Authority. “BC Hydro 2008 Annual report.” March 2009: <http://www.bchydro.com/about/company_information/reports/2008annualreport/intro.html>.

51. Lilliefors, H.W., "On the Komogorov-Smirnov test for normality with mean and variance unknown," Journal of the American Statistical Association, 62 (1967): 399-402.

52. Lial, Kelly. EPCOR. Personal communication. September 2008.

53. US Energy Information Administration. “Assumptions to the Annual Energy Outlook 2009. Report #: DOE/EIA-0554(2009).” March 2009. http://www.eia.doe.gov/oiaf/aeo/assumption/index.html

Appendix A – Theoretical Wave Power Calculations

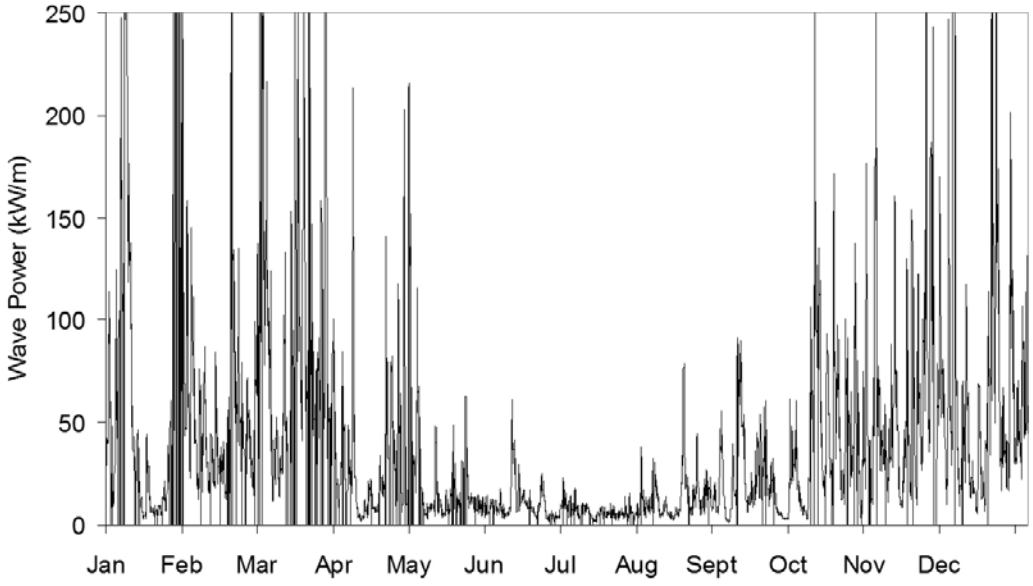

Figure 56: West Dixon Entrance hourly theoretical wave power for 2000

Peak Wave Power: 919 kW/m

Annual mean Wave Power: 42 kW/m

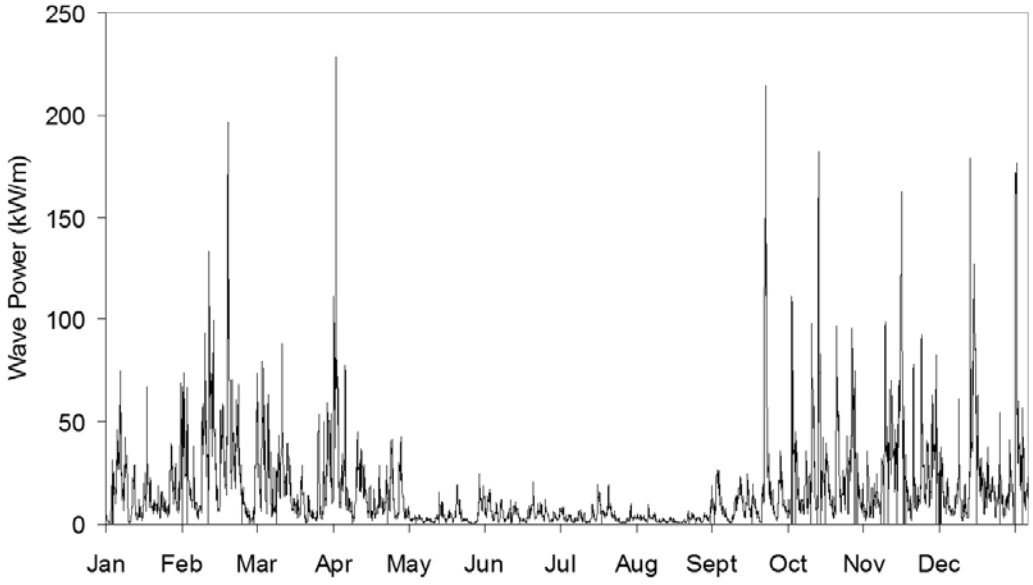

Figure 57: Central Dixon Entrance hourly theoretical wave power for 2005

Peak Wave Power: 229 kW/m

Annual Mean Wave Power: 16 kW/m

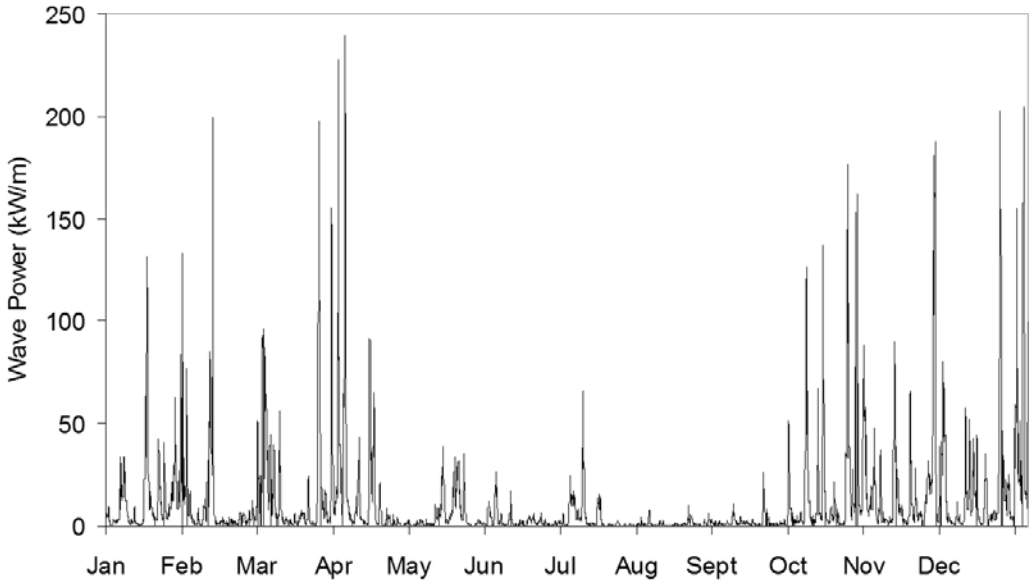

Figure 58**:** North Hecate Strait hourly theoretical wave power for 2005

Peak Wave Power: 240 kW/m

Annual Mean Wave Power: 11 kW/m

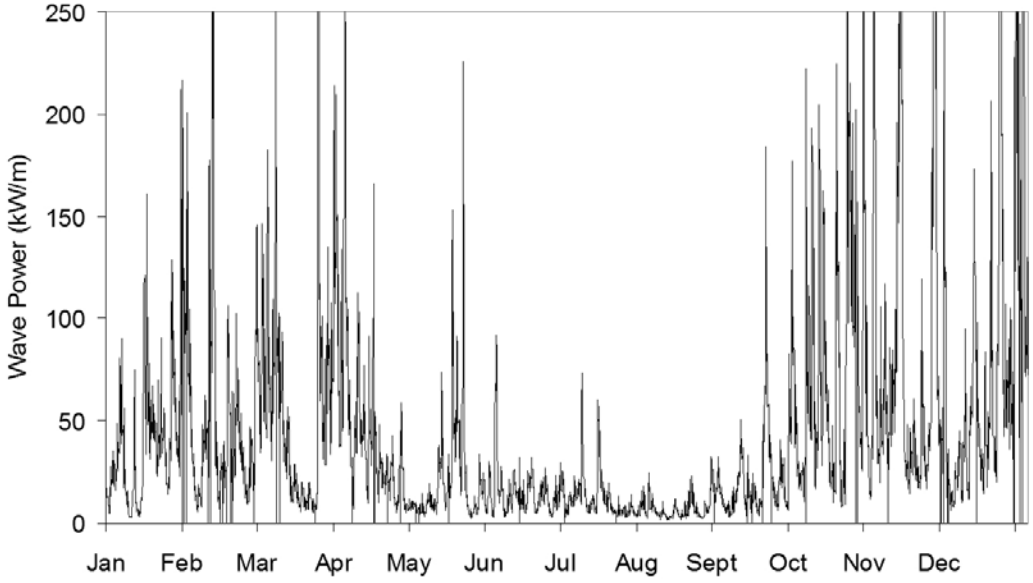

Figure 59: South Moresby hourly theoretical wave power for 2005

Peak Wave Power: 681 kW/m

Annual Mean Wave Power: 43 kW/m

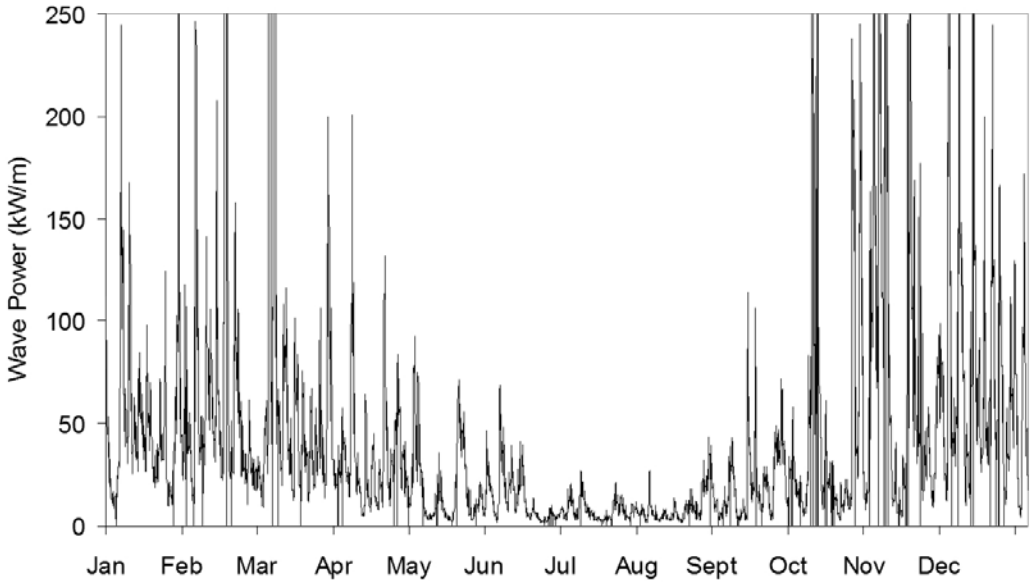

Figure 60: West Moresby hourly theoretical wave power for 2004

Peak Wave Power: 752 kW/m

Annual Mean Wave Power: 42 kW/m